Molar Volume Mismatch: a Malefactor for Irregular Metallic Electrodeposition in Solid Electrolytes

Aashutosh N. Mistry[1†] and Partha P. Mukherjee[2*]

School of Mechanical Engineering, Purdue University, West Lafayette, IN 47907, United States

TOC Graphic

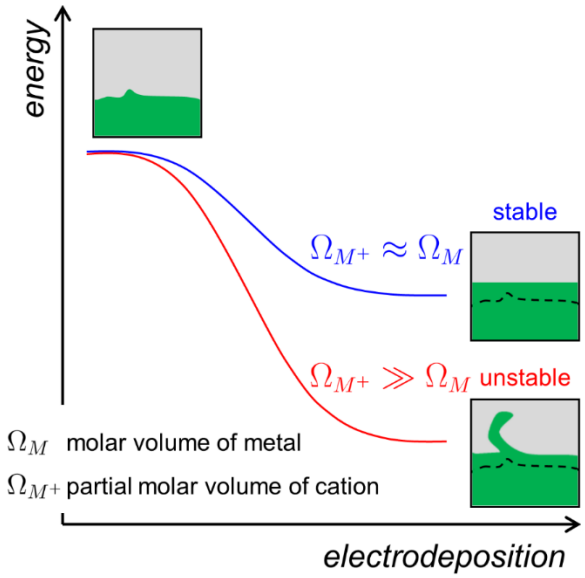

Non-equilibrium thermodynamics reveals a low energy path of localized electrodeposition with solid electrolytes when the molar volumes of interacting species are inequal.

Highlights

i. An energy-based mechanism explaining irregular electrodeposition is identified
ii. Large cationic molar volume favors localized (irregular) growth
iii. Stability varies non-monotonically with electrolyte stiffness
iv. Stress-assisted ionic transport can stabilize irregular growth

* Email: pmukherjee@purdue.edu
† present address: Argonne National Laboratory, United States
[1] ORCID: 0000 – 0002 – 4359 – 4975
[2] ORCID: 0000 – 0001 – 7900 – 7261

Abstract

Regularizing metallic electrodeposition has been a long-standing challenge in energy storage. Leveraging mechanical stresses, solid ion conductors have been proposed to stabilize the evolving interface. Paradoxically softer electrodepositing metals are often found to form penetration fronts under the hypothesized stable conditions. We find that mechanical contributions to energy of the interacting species (i.e., metal and cation) relate to respective molar volumes. The stresses at the electrodepositing interface are correlated, and consequently, localized deposition is energetically favored for larger cationic molar volumes. Electrolyte stresses cause a stress-driven ionic flux away from compressed locations, which proves to be a stabilizing influence. Stability is found to be nonlinearly related to electrolyte stiffness. Material complexities such as interphases, interlayer, and grain boundaries are also examined to proffer guidelines for a stabilized growth.

Keywords

i. Metal anode
ii. Solid electrolyte
iii. Molar volume
iv. Electrochemical potential
v. Non-equilibrium thermodynamics
vi. Reaction distortion
vii. Transport distortion
viii. Electrolyte stiffness
ix. Wetting

Context & Scale

The solid electrolytes are advocated to be a transformative element for the next-generation energy storage systems given the promises of thermal stability, non-volatility, leakage-free nature and the potential for mechanically-assisted stabilization of metallic anodes. However, various solid electrolytes have at best been marginally successful in regularizing the unstable irregular growth of the electrodepositing interface. We identify the fundamental mechanism responsible for this otherwise mysterious behavior. This mechanistic discovery and renewed understanding of the generalized dynamical interactions in solid electrolytes provide a rational basis for future improvements in metal batteries.

Introduction

The elegance of metallic anodes, e.g., lithium, magnesium, aluminum, emanates from apparently simplistic interactions, namely, highest specific energy (entire phase is active),

extreme reactivity (minimal kinetic resistance), metallic nature (negligible electron conduction limitation) and elementary electrodeposition reaction (unlike more complex solid-state intercalation[1] or mixed solid-liquid conversion kinetics that causes speciation-driven complexations[2-3]). However, fast or repeated electrodeposition degenerates to a characteristic spatiotemporal nonuniformity, more commonly referred to as the electrodeposition instability. The fundamental origins of the causality between off-equilibrium functioning and the electrodeposition instability have been a focus of scientific investigations[4-13]. Given the mechanically compliant nature of the conventional liquid electrolytes, it has been hypothesized that stiff solid ion conductors should provide a balancing influence to regularize the electrodeposition phenomenon[14-22]. Surprisingly, the experimental findings have been unexpected[23-40] and reveal that contrary to the monotonic belief, the stress-interactions are non-simpleton (section S1 provides a detailed discussion of representation works).

Consider an electrodepositing metallic electrode in contact with a solid electrolyte as shown in Figure 1(a). In the absence of any inhomogeneity along the electrochemical interface, one would expect fresh deposition to occur as a planar front (this is the desired growth mode). If the underlying material interactions are stable, any perturbation to the growing interface would be attenuated, and the interface gradually becomes planar. Figure 1(b) exemplifies time evolution of the perturbed interface for stable growth. Alternatively, unstable interactions would amplify the initial disturbance and the interface evolves towards a non-planar shape (Figure 1(c)). As the growth is caused by electrodeposition reaction, corresponding current distributions differ qualitatively between Figure 1(b) and (c). During the stable growth, peak locations grow slower than the average deposition front, and the valley locations grow faster such that over time growth rates of all the interface locations match. Unstable growth represents an opposite situation, where a successively greater amount of reactions take place at the protrusions, in turn, growing them in an accelerated fashion.

Unstable growth is a characteristic of destabilizing interaction(s). Instabilities are often found in systems marked by multiple transport processes[41-42], for example, dendrite formation during melt solidification[43-44]. An electrochemical system functions on kinetic (short-range) and transport (long-range) interactions[45]. For metallic electrodeposition in liquid electrolytes, ionic transport is the destabilizing influence wherein irregular growth is favored when depositing ions do not reach all the reaction sites and the ones with sufficient ionic concentration grow selectively[4-5, 7]. An unstable deposition is also observed when solid electrolytes are employed[23, 31, 34-35, 46]. Of these inorganic solid electrolytes are of particular interest given their higher stiffnesses. Unlike liquid and polymer electrolytes containing salt (i.e., anion and cation) in a solvation environment, these inorganic ion conductors contain crystal structures wherein metallic ions, M^+, move through a (stationary, negatively charged) lattice[47-50]. Charge neutrality is ensured over the length of a unit cell, and the local M^+ concentration is fixed by the stoichiometry of the electrolyte composition. Thus, ionic concentration is predetermined during electrolyte preparation, and not affected by passage

of current as one would expect in a liquid or a polymer electrolyte (if multiple stoichiometric phases exist in an electrolyte sample, ionic concentration would vary locally to satisfy stoichiometry and charge neutrality, and reflect in ionic conductivity differences among these phases; however, the concentration would not vary in time in response to an ionic current). Given the ionic availability, electrodeposition instability similar to liquid electrolytes cannot manifest, and further ambiguates the origins of electrodeposition instability in these electrolytes.

During planar growth, solid electrolyte slowly moves with a velocity, $v = \Omega_M i_{\mathrm{app}}/F$, where the fresh metal deposits at current density, i_{app} (in a similar setting, a liquid electrolyte experiences a bulk flow velocity of similar magnitude). Such growth takes place with a negligible deformation of the electrolyte, and mechanical stresses are fairly uniform throughout. If the fresh metal deposition is nonuniform (Figure 1(d)), metal – electrolyte interface locations displace by different amounts. The unequal displacements cause strains in solids which in turn generate mechanical stress gradients. Mechanical stresses are conservative forces and contribute to the energy of different phases and species involved. If the system evolution were purely governed by mechanical energy changes, the gradual transition would be to a gradient-free state. However, in the presence of multiple material interactions (Figure 1(d)), non-unique equilibrium states exist (non-equilibrium thermodynamics is a paradigm to examine such transitions of a complex system).

The stress gradients change the (free-)energy of both cation, M^+, and metal, M, per the relations, $\delta\mu_{\mathrm{M}^+} = -\Omega_{\mathrm{M}^+}\delta\sigma_{\mathrm{h},e}$ and $\delta\mu_{\mathrm{M}} = -\Omega_{\mathrm{M}}\delta\sigma_{\mathrm{h},M}$[51-53]. Stress field is made up of volume-changing (i.e., hydrostatic) and shape-changing (i.e., deviatoric) components. Changes in volume microscopically vary the mean distance between species and are predominantly responsible for energy changes of atoms and corresponding cations (e.g., Li and Li^+)[51-52]. Such species are referred to as isotropic solutes, and the volume-changing contribution of the stress field is often called hydrostatic stress. For more complex (molecular) solutes, e.g., Li_2S in solid electrolyte[54], even shape-changing stresses cause energy changes via microscopically altering orientations of molecules and/or its atomic constituents (rotation and stretching of bonds). Such an effect is expected to be more pronounced in asymmetric molecules. For the present discussion, given the microscopic isotropicity of interacting species, hydrostatic stress contributes to energy changes. Here the hydrostatic stress refers to the volume-changing stress component, and the overall stress state need not be purely hydrostatic (a purely hydrostatic stress state is a condition of uniform pressure acting along all the directions[55-57]).

Aforementioned mechanical contributions to (free-)energy alter reaction and transport signatures (section S3 and S6, respectively; Figure 1(d)). For instance, the energy of cations in compressive locations is higher (due to smaller mean separation microscopically) and a macroscopic drive exists to transfer ions from compressive to tensile locations. Such a stress-driven current is in addition to the conventional ohmic current

caused by electric field gradients. Mathematically, ionic current in solid single-ion conductors is:

$$i = -\kappa \nabla \phi_e - \kappa_\sigma \nabla \sigma_{\mathrm{h}} \qquad (1)$$

Compressive stresses are negative and tensile stresses are positive. The stress conductivity, κ_σ, is negative (section S6). Hence, the term $-\kappa_\sigma \nabla \sigma_{\mathrm{h}}$ refers to the current flow from compressive to tensile locations (the negative κ_σ is not unusual; in a concentrated solution theory treatment, diffusional conductivity, κ_D, is a negative property as well[45, 58]). A recent study documents the existence of stress-driven ionic transport in a solid ion conductor[59].

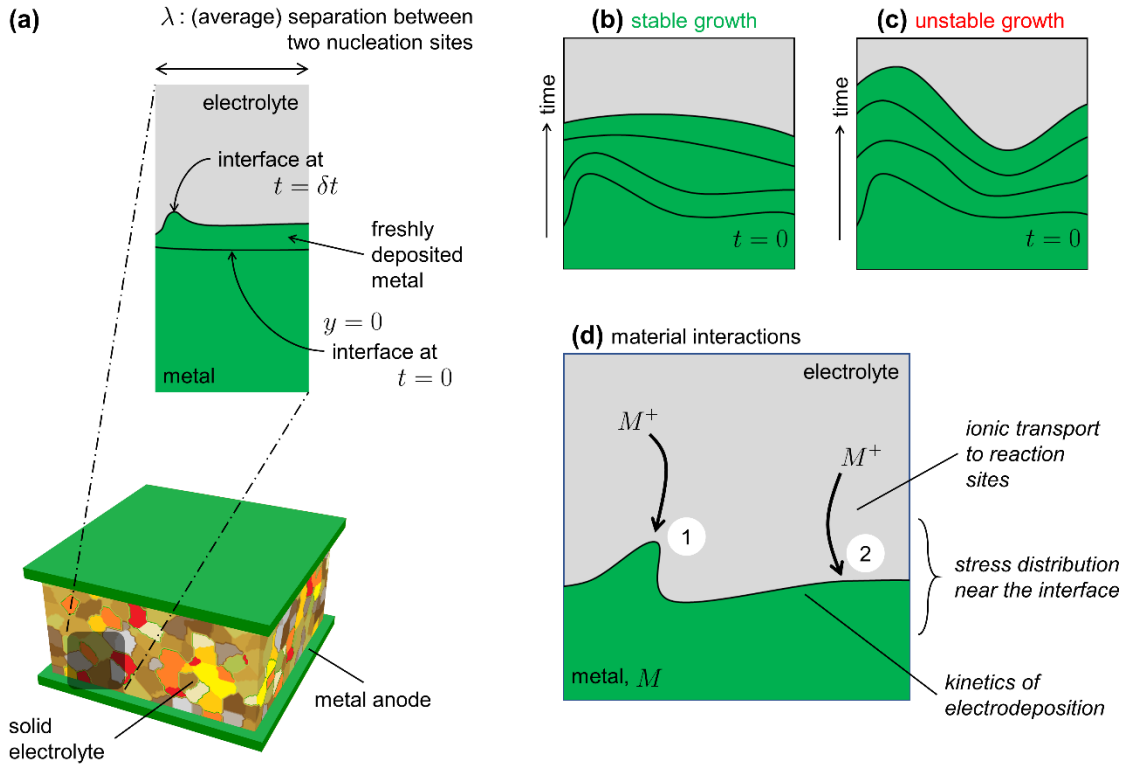

Figure 1. Material interactions during irregular electrodeposition: (a) schematic of depositing metal – electrolyte interface in a metal | solid electrolyte | metal symmetric cell; (b) stable and (c) unstable growth of electrochemical interface; (d) mechanical stresses and electric fields jointly govern interface evolution.

The mechanical stresses introduce an asymmetry in electrodeposition reaction, $M \underset{\text{deposition}}{\overset{\text{dissolution}}{\rightleftharpoons}} M^+ + e^-$ (in general, M can form a multivalent cation, M^{n+}, and such an extension is trivial) wherein the formation of a cation brings in a mechanical energy change, $\Delta\mu_{\text{mechanics}} = -\Omega_{M^+}\sigma_{\mathrm{h},e} + \Omega_M \sigma_{\mathrm{h},M}$. If $\Delta\mu_{\text{mechanics}} > 0$, dissolution is unfavored, and an intrinsic tendency for localized deposition exists. Appropriate kinetic expression (section S3) is:

$$i_{rxn} = i_0 \left\{ e^{F\eta_{\text{mechanics}}/RT} e^{F\eta_{\text{electric}}/2RT} - e^{-F\eta_{\text{electric}}/2RT} \right\} \quad (2)$$

where mechanical bias, $\eta_{\text{mechanics}} = \eta_\sigma = \left(\Omega_{M^+}\sigma_{\text{h},e} - \Omega_M \sigma_{\text{h},M}\right)/F$. The bias due to electric field, $\eta_{\text{electric}} = \eta_\phi = \phi_s - \phi_e - U$, is the conventional overpotential.

Spatiotemporal evolution of an electrodepositing interface (Figure 1(d)) is thus governed by mechanical stresses generated due to irregular growth and their interplay with ionic transport (Eq.(1)) and reaction kinetics (Eq.(2)). For such asymmetric interactions to trigger, some form of interfacial inhomogeneity is required. Material inhomogeneity[31] is one such culprit, but it can, in principle, be ameliorated by careful sample preparation. On the other hand, thermal fluctuations are universally present and inherently cause microscopic differences in reaction rates (stability analysis in a traditional setting mimics such a perturbation as an interfacial displacement with varying wavelengths[15, 60-61]). However, at small lengthscales representative of an electrodepositing interface, nucleation sites become relevant[4, 62]. Consequently, lengthscale of interfacial inhomogeneity relates to the average separation between nucleation sites (Figure 1(a)). The stochastic thermal fluctuations dictate the spatial distribution of nucleation events as well as the specific time sequence of nuclei appearance. When electrodeposition is repeated under identical operating conditions, nuclei grow at different locations, but the average characteristics, e.g., average separation, remain invariant.

Herein we examine the electrodeposition stability of lithium growth in a solid single-ion conductor. Stress contributions to electrochemical interactions are assessed in a non-equilibrium thermodynamics setting. We identify the mismatch of molar volumes in the two adjoining phases to be fundamentally responsible for the observed instability. In addition to accounting for seemingly non-congruent experimental observations, the present study articulates rules for material selection and modification.

Results and Discussion

Electrodeposition is made up of (i) formation of discrete nuclei (ii) growth of nuclei and (iii) continuous growth of active interface. Each of these stages is characterized by specific dynamical interactions, for example, nucleation is largely governed by interfacial energies[44]. The present discourse analyzes the stability of continuous growth where the asymmetry in interfacial deposition relates to nucleation and growth history (hence the corresponding lengthscale, λ). As shown in Figure 2(a), fresh deposition takes place over a small time instant, δt. This time is small enough compared to the timescale of continuous growth but large enough compared to nuclei growth.

Such an occurrence of new lithium generates stresses in the electrolyte as well as preexisting lithium (section S2). Figure 2(b) presents stress fields in lithium and solid electrolyte with an LLZO like stiffness $(G_e = 60\ \text{GPa})$. The fresh deposition displaces metal – electrolyte interface nonuniformly. In turn, compressive (negative) stresses are generated

near more deposition, and less deposited locations experience tension. The stress field in solid electrolyte subsequently generates stresses in lithium. Since lithium is softer than LLZO $(G_{Li} = 4.2\ \text{GPa} \ll G_e = 60\ \text{GPa})$, relatively greater strains are generated in lithium. Equivalently, volumetric changes and hydrostatic stresses are larger in lithium (Figure 2(b)). Iso-contour lines are shown to aid visualization. Figure 2(d) presents interfacial hydrostatic stresses for both the materials (normal and shear stresses are balanced at the interface; however, corresponding hydrostatic stresses can differ). Interfacial hydrostatic stress in lithium follows the general trend in electrolyte stress. However, maximum hydrostatic stresses in the two materials do not coincide, in part due to shear stress distribution. Electrolyte stresses conform to fresh deposition profile and maximum compressive stress occurs at the highest deposition point (equivalent maximum tensile stress occurs at the lowest deposition thickness). Interfacial shear stress is greatest wherever deposition thickness varies strongly. Since lithium stresses are defined by both normal (highest at peak locations) and shear (highest in between) electrolyte stresses, its hydrostatic stress profile differs (Figure 2(d)).

Mechanical bias to reactions, η_σ, relates to molar volumes of interacting species. Molar volume of a pure phase (here Li) is well-defined, however, it is difficult to measure for ionic species, especially in single-ion conductors (refer to section S4 for a debate on its interpretation). Alternatively, values for Ω_{Li^+} are assumed. Liquid electrolyte measurements[15] suggest that $\Omega_{Li^+} > \Omega_{Li}$, and a dimensionless descriptor, $\psi_r = \Omega_{Li^+}/\Omega_{Li}$, is defined to explore its effect. Since both the volumes appear in reaction expression (Eq. (2)) and scale the effect of stress-induced asymmetry, ψ_r is termed 'reaction distortion'. Figure 2(e) outlines the stress overpotential, η_σ, variations in response to the new deposition (here $\psi_r = 5$), and shows that for $\Omega_{Li^+} > \Omega_{Li}$, generated mechanical stresses bias reactions towards the formation of new lithium. In energetic terms, large Ω_{Li^+} increases cation energy in compressive locations such that energy can be released by locally forming more Li at the expense of Li^+ from the electrolyte.

Stress-driven transport, i.e., $-\kappa_\sigma \nabla \sigma_\text{h}$ term in Eq. (1) counters this tendency. If this regularizing influence is not strong, reaction distribution skews towards more deposited locations as shown in Figure 2(f)unstable. Figure 2(c) shows electrolyte potential distribution, along with ionic current vectors. When the stress-driven transport is weak (as stress fields relate to stiffness, for a given electrolyte, strength of this term scales with stress-conductivity, κ_σ), current vectors are (partially) aligned with gradients in electrolyte potential, ϕ_e, as shown in Figure 2(c)unstable. Alternatively, when this effect is stronger, vectors (partially) align with stress gradients. Concurrently, reaction distribution switches (Figure 2(f) unstable vs. stable). Partial alignment originates from the two competing influences in ionic current (Eq.(1)). If the stress conduction were absent $(\kappa_\sigma = 0)$, the ionic flux will align strongly along the electrolyte potential gradients.

If more reactions coincide with $(i_{rxn}/i_{\text{app}} > 1)$ where more deposition took place initially, over time, it will grow faster than the adjoining locations and lead to unstable

growth as schematically shown in Figure 1(c). A dimensionless stability quotient, Θ, using the slope of the reaction current distribution, i_{rxn}, is defined to quantify such a preference. Stable deposition implies a faster growth of less deposited locations and exhibit $\Theta > 0$. Alternatively, $\Theta < 0$ marks unstable growth. When reaction distribution is uniform, every location grows equally and $\Theta = 0$. The stability quotient, Θ, can be interpreted as a correlation coefficient characterizing the similitude of deposition and reaction profiles. If the two are correlated, unstable growth results $(\Theta < 0)$. If the two are anticorrelated, interface evolution is stable $(\Theta > 0)$. When the two are uncorrelated, electrodeposition is neutrally stable $(\Theta = 0)$.

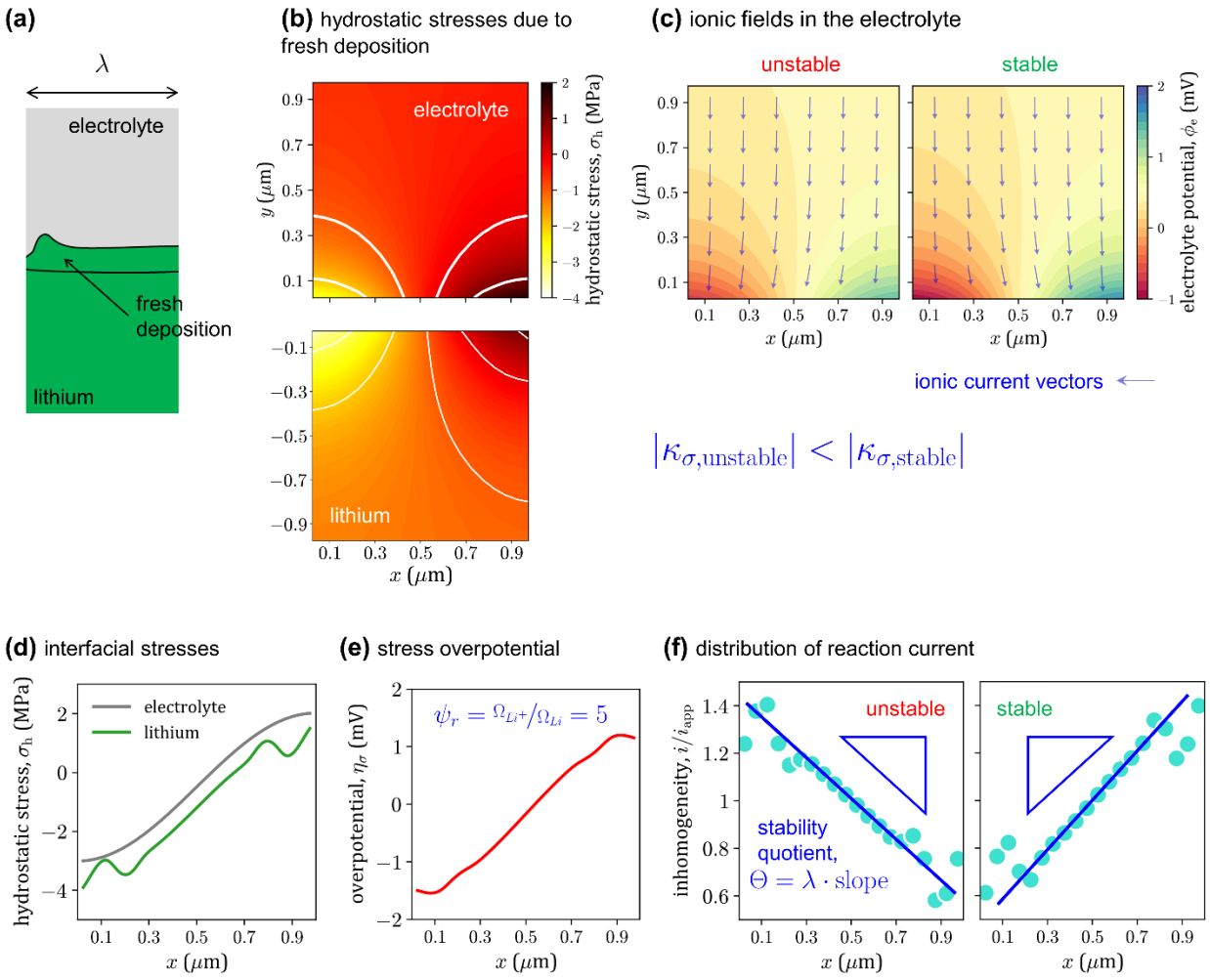

Figure 2. Origins of unstable electrodeposition: (a) schematic of the electrodepositing interface; (b) distribution of the hydrostatic stress; (c) ionic current and electrolyte potential in electrolyte; (d) hydrostatic stresses at the interface; (e) mechanical overpotential; (f) reaction current distribution for lithium electrodepositing against an LLZO like electrolyte. Stress-assisted ionic flux can counter local deposition preference and in turn, stabilize growth.

There are non-monotonic features in the deposition current (Figure 2(f)), whose origin can be tracked to interfacial stress profiles (Figure 2(d)). Such characteristic local extremum points (Figure 2(f)) act as growth locations leading to primary and secondary branches as observed recently[35] in inorganic solid electrolytes. As mentioned earlier, irregular growth is observed in many different settings; however, the geometry of growth (referred to as morphology) varies considerably. For example, melt solidification in traditional metallurgy[63] forms characteristic pine tree patterns, while unstable electrodeposition in liquid electrolytes[4-5, 8] resembles an oak tree. These differences are an outcome of the underlying diversity of interactions.

Electrodeposition Stability Map

As discussed in Figure 2, large cationic partial molar volume causes a spontaneous (energetic) preference for localized irregular growth. Such an intrinsic preference is countered by stress-driven ionic transport. Put simply, mechanical contribution to the reaction kinetics can cause irregular growth. The electrolyte transport is the stabilizing influence (e.g., Figure 2(c)). Both these effects, the mechanical bias for deposition and stress-assisted ionic transport, relate to partial molar volume of cations (section S3, S6) which are difficult to measure. The values of Ω_{Li^+} in liquid and polymer electrolytes[15-16] are reported to be about ten times that of lithium metal. Secondly, the stress conductivity is related to ionic conductivity via cationic molar volume as $\kappa_\sigma = {}^{-\kappa\Omega_{Li^+}}/_{F}$ (Eq. (S29), section S6). Note that Ω_{Li^+} appearing in kinetic expression (Eq. (2)) is a solid electrolyte property at the interfacial contact, and may differ from its bulk value (defines transport in Eq. (1)). Unlike a solid-liquid interface, solid-solid contact is not necessarily conformal. Hence, the microscopic order can differ at the interface as compared to its bulk nature, resulting in different cationic partial molar volumes near the surface and in the bulk. To account for such differences, a dimensionless descriptor, $\psi_t = {}^{\Omega^{\text{bulk}}_{Li^+}}/_{\Omega^{\text{interface}}_{Li^+}}$, is defined. Since it relates to stress-driven ionic transport (a departure from ohmic ionic transport), it is termed as 'transport distortion'. ψ_t expression can be simplified to $\psi_t = {}^{-F\kappa_\sigma}/_{\kappa\Omega^{\text{interface}}_{Li^+}}$. In the absence of explicit measurements for inorganic solid electrolytes and based on limited data in other electrolyte systems, we assume that the reaction distortion, $\psi_r = {}^{\Omega_{Li^+}}/_{\Omega_{Li}}$, varies between 1 and 10. The transport distortion, $\psi_t = {}^{-F\kappa_\sigma}/_{\kappa\Omega_{Li^+}}$, is assumed to vary between 0.1 and 1.

Figure 3(a) examines the electrodeposition stability of an LLZO like electrolyte $(G_e = 60\ \text{GPa})$ on a distortion coordinates map (ψ_r, ψ_t). Note that mechanical fields are set based on the amount of deposited lithium, and are independent of (ψ_r, ψ_t) in the present context (in general, new deposition profile is determined by (ψ_r, ψ_t), which causes a new stress field and the interface evolves accordingly; such dynamic evolution is not studied here). For negligible transport – mechanics interplay $(\psi_t = 0.1)$, mechanical stresses are generated such that even a slight mismatch in molar volumes, $\Omega_{Li^+} > \Omega_{Li}$, triggers localized electrodeposition (with a stiff LLZO like electrolyte). The electrodeposition becomes more

localized as molar volume inequality grows and reflects in more negative stability, Θ. As transport – mechanics interplay becomes stronger, the stability improves (i.e., a wider range of cationic volumes are stable). For larger transport distortion, ψ_t, moderately dissimilar molar volumes do not trigger localized deposition since the stresses can effectively divert the ionic flux from compressive (i.e., more deposition) locations. A neutral stability curve $(\Theta = 0)$ is shown in Figure 3(a) that marks uniform current distribution and growth such that the initial perturbation neither amplifies nor attenuates in time.

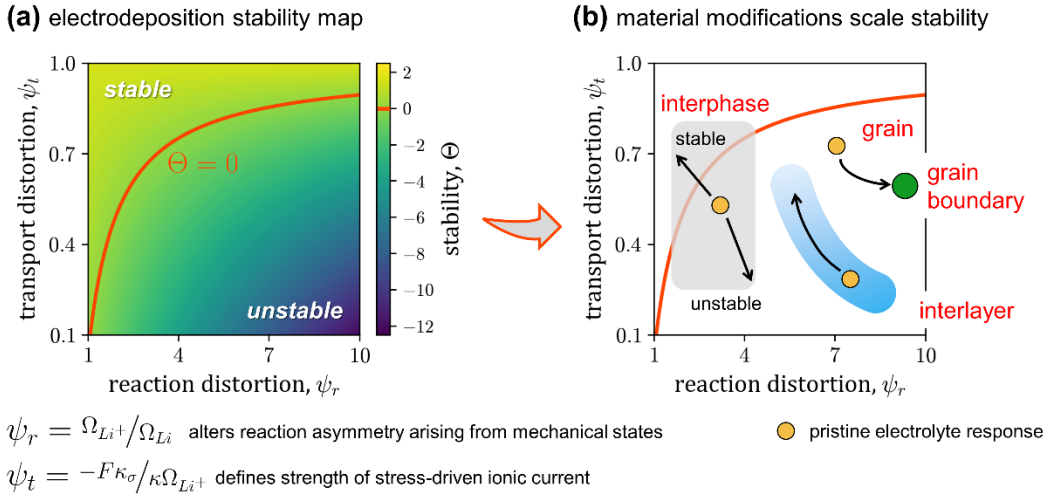

Figure 3. Electrodeposition stability: Mechanical stresses introduce an asymmetric bias in reaction (reaction distortion) and divert ionic current (transport distortion) from compressive locations. (a) An electrodeposition stability map represented in distortion coordinates for an LLZO like electrolyte $(G_e = 60\ \text{GPa})$; (b) Effect of material modification on stability.

Structural Modifications

Electrodeposition stability as interpreted in terms of distortion coordinates (Figure 3(a)) also allows one to rationalize implications of material complexities such as interphases, interlayers and grain boundaries (Figure 3(b)). Interphase is a few microns thick $(\sim 10\ \mu\text{m})$ material domain that is structurally different than bulk solid electrolyte. It could result from the chemical reactivity of the electrode-electrolyte interface[40] or be artificially introduced[36]. Since the thickness is comparable to nucleation site separation, λ, it contributes to both interfacial and bulk interactions. If the cationic molar volume is higher in an interphase material, it causes a higher spontaneity for localized deposition. It could partly be offset by stress-assisted transport. A good interphase material should exhibit negligible reaction distortion $\left(\Omega_{Li^+}^{\text{interface}} \to \Omega_{Li}\right)$ to decrease the thermodynamic tendency for irregular growth and high stress conductivity $\left(\Omega_{Li^+}^{\text{bulk}} \to \Omega_{Li^+}^{\text{interface}}\right)$ to divert ionic current from high deposition locations. In other words, an effective interphase material has a negligible mismatch of molar volumes, i.e., $\Omega_{Li^+}^{\text{bulk}} \sim \Omega_{Li^+}^{\text{interface}} \sim \Omega_{Li}$. Experimentally, interphases are found to demonstrate

an ambiguous effect on growth morphology[36, 40]. An interphase material showing stable[36] growth is likely to exhibit $\Omega_{Li^+}^{\text{bulk}} \sim \Omega_{Li^+}^{\text{interface}} \sim \Omega_{Li}$, while the one demonstrating unstable[40] growth possibly displays $\Omega_{Li^+}^{\text{bulk}} \ll \Omega_{Li^+}^{\text{interface}}$ and/or $\Omega_{Li^+}^{\text{interface}} \gg \Omega_{Li}$. Figure 3(b) schematically highlights the stabilizing and destabilizing contributions of interphase. Pristine electrolyte condition is also marked.

An interlayer is a thin $(\sim 5\ \text{nm})$ material layer expected to engineer a conformal physical contact for an otherwise non-conformal solid-solid interface between lithium and solid electrolyte. It is expected to behave as a conduit for flux transport (commonly used for reducing contact resistance against heat flux or electrical current across two solids[64]). Small thickness does not alter the bulk interactions but affects reaction kinetics via altering the cationic molar volume. On the electrodeposition stability map, this amounts to traversing along $\psi_r \cdot \psi_t = \text{constant}$ curve (Figure 3(b)) and improves stability via decreasing the cationic molar volume at the interface as compared to solid electrolyte, i.e., $\Omega_{Li^+,\text{interlayer}}^{\text{interface}} < \Omega_{Li^+,e}^{\text{interface}}$. In terms of distortions, an interlayer reduces reaction distortion and enhances transport distortion, both of which favor stable deposition. This interpretation explains the (somewhat mysterious) positive role of interlayers as found experimentally[27, 29, 65-67], even with materials whose bulk interactions with lithium are known to be catastrophic, e.g., silicon and germanium[68-69].

Alternatively, the solid electrolyte can contain material inhomogeneities that would manifest as local differences in relevant properties such as reaction rate (i.e., exchange current density, i_0), cationic molar volume, ionic conductivity, stiffness, etc. Of different inhomogeneities, grain boundaries are particularly interesting. A characteristic observation in inorganic polycrystalline electrolytes has been filament propagation along the grain boundaries[23, 35]. The grain boundaries represent a state of disorder (and high energy) as compared to the bulk crystals, which is expected to give rise to a higher cationic molar volume. The higher partial molar volume, Ω_{Li^+}, makes localized deposition more favorable compared to grains, i.e., bulk electrolyte (Figure 3(b)). These structural variations also modify the mechanical response due to differing stiffnesses. Consequently, the usefulness of such additional phases is to be assessed by collectively examining molar volumes and stiffnesses.

Stiffness Aberrations

The present analysis estimates the mechanical state of the lithium and electrolyte phases when a prescribed amount of fresh deposition takes place. Subsequently, the generated stresses describe the electrochemical fields. Such a sequential approach provides information about static stability, i.e., the intrinsic material tendency to promote unstable growth. Figure 2 and Figure 3 discuss electrodeposition with an LLZO like $(G_e = 60\ \text{GPa})$ solid electrolyte. Figure 4 summarizes equivalent predictions with different electrode stiffnesses. Figure 4(a) presents neutral stability curves $(\Theta = 0)$ for four representative solid

electrolytes and reveal that the qualitative nature of stability is equivalent for different electrolytes. More interestingly, Figure 4(a) shows that the stability window (i.e., region with positive Θ) expands when stiffness is reduced from 60 GPa (LLZO like) to 10 GPa (LPS like), shrinks for 4.2 GPa (comparable to lithium) and eventually expands for 1 GPa (softer than lithium) electrolyte. Such a non-monotonic response is summarized along a diagonal axis, named critical distortion, ψ^*. The diagonal axis combines the influence of mechanical interplay with reaction and transport signatures. Figure 4(b) provides a more detailed variation of stability with stiffness in terms of the critical distortion. The critical distortion values in Figure 4(b) refer to intersection points of ψ^* coordinate and neutral stability $(\Theta = 0)$ curve for each electrolyte in Figure 4(a). Such intersection points are marked for visual identification in Figure 4(a). Critical distortion quantifies the requisite stress-assisted conduction to counter the energetic tendency for localized deposition due to molar volume mismatch $(\Omega_{Li^+} > \Omega_{Li})$. For example, $\psi^* \to 0$ relates to strong mechanical – transport effect to counter stress-induced asymmetry in reaction kinetics. Alternatively, $\psi^* \to 1$ identifies a small need for stress-driven transport to stabilize reactions. In other words, $\psi^* \to 1$ is intrinsically more stable as the mechanical asymmetry in reactions is negligible (note that reaction kinetics is the destabilizing influence in this system). On the other hand, $\psi^* \to 0$ is highly unstable since even a small molar volume mismatch leads to considerable imbalance such that strong transport distortion is required to invalidate asymmetric reaction.

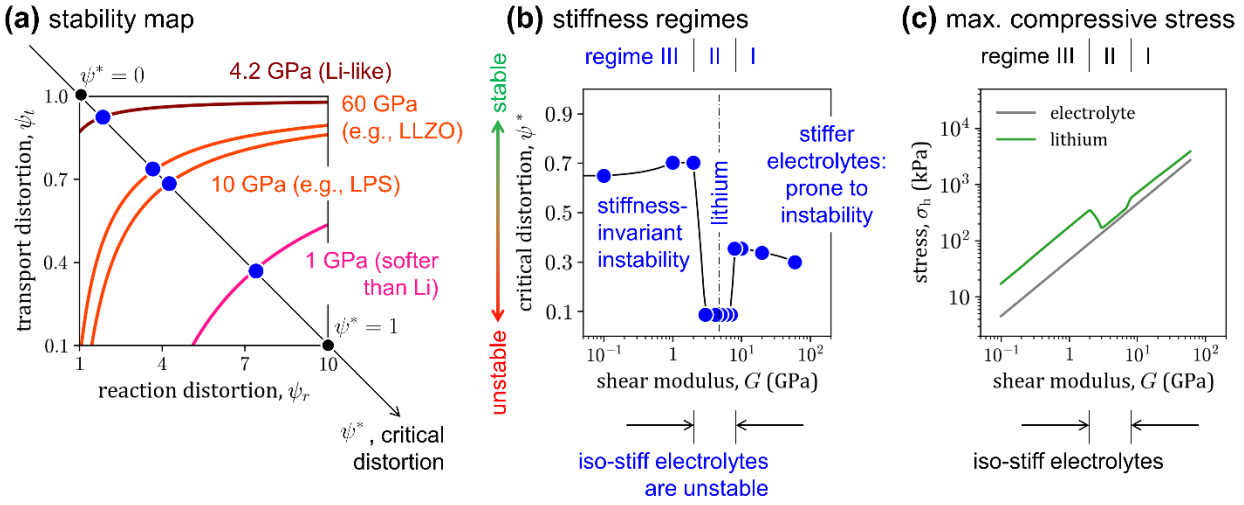

Figure 4. Role of electrolyte stiffness: (a) neutral stability $(\Theta = 0)$ curves for different stiffness electrolytes as shown on a stability map; (b) critical distortion variations with electrolyte stiffness; critical stiffness defines intrinsic stability with higher values signifying better stability; (c) maximum compressive stresses in electrolyte and lithium for different electrolyte stiffnesses.

Three stiffness regimes emerge in Figure 4(b). Regime I refers to electrolytes stiffer than lithium $(G_e \gtrsim 2G_{Li})$ where stiffer electrolytes gradually become less stable towards irregular growth. The second regime is made up of electrolytes that are comparable to

lithium $(2G_{Li} \gtrsim G_e \gtrsim {}^{G_{Li}}/_{2})$ and exhibit minimal stability. Regime III describes softer electrolytes $(G_{Li} \gg G_e)$ and demonstrates higher stability (even higher than regime I). Typical inorganic electrolytes like LLZO and LPS fall in regime I, while (organic) polymer electrolytes represent regime III. Such trends considerably differ from previous theoretical studies[15-17, 19] but quite faithfully account for experimental trends. Experimentally, LPS (~10 GPa) is found to resist irregular deposition more than LLZO (~60 GPa)[35] as predicted in regime I; and much softer polymer electrolyte does not experience mechanically-destabilized uncontrolled growth[31] (refer to section S7 for a mechanistic discussion on experiments[31]). The difference in theoretical treatment arises from a non-equilibrium treatment of material interactions that account for the peculiarities of the solid structure, rather than modifying liquid electrolyte relations to interpret stability[15-17, 19].

As argued earlier (Figure 1(c)), the mechanical bias for deposition primarily relates to the distribution of compressive stresses. Figure 4(c) plots the variations of maximum compressive hydrostatic stresses (i.e., most negative value) in lithium and electrolyte as electrolyte stiffness is varied. Since electrolyte deforms elastically, for the same deposition profile in time δt, stress field scales linearly with stiffness. Hence, electrolyte stress shows a trivial variation in Figure 4(c). The stress field in lithium is, however, more complex (Figure 4(c)). When two materials with very different stiffness are in contact, large strains are generated in a softer material. The strain field in electrolyte relates to the electrodeposition profile, while lithium strains scale with the ratio of their stiffnesses $({}^{G_e}/_{G_{Li}})$. Hence, in regime I, lithium experiences large strains, while in regime III, strains in lithium are smaller compared to the electrolyte. In these regimes (I and III), volumetric changes scale with strains. As stiffness increases in regime I, stress magnitude increases which in turn leads to a greater mechanical bias towards deposition, $\Delta\mu_{\text{mechanics}}$. Hence, stability deteriorates with stiffness in regime I. When the electrolyte is very soft, not enough stresses are generated and mechanically-induced asymmetry is minimal. Hence, stability in regime III is better than regime I. As stiffness is increased in regime III, stress-assisted transport becomes more significant and accounts for a slight improvement in stability for regime III. As stiffness is decreased gradually from regime I to II, lithium strains become comparable to the electrolyte. In the regime II, deformations in both materials are of similar magnitudes (unlike I and III where one material deforms quite extensively) and in turn, volumetric changes are comparable and the lithium stresses reduce to be similar to the electrolyte. Another such transition is observed when stiffness is further reduced such that electrolyte experiences large volume change. In other words, when lithium deposits against a stiff electrolyte (regime I), new lithium is accommodated by large volumetric strains in lithium. When lithium deposits against a soft electrolyte (regime III), fresh lithium is predominantly acclimatized via volume change of the soft electrolyte. Alternatively, when stiffnesses are similar, i.e., iso-stiff electrolytes in regime II, the electrodeposited phase is partly housed in both the phases with relatively moderate volumetric strains in either of the materials and comparable stresses.

The regimes in Figure 4(c) should be interpreted carefully. The higher stability of regime III originates from a comparatively smaller mechanical bias for the deposition that can be regularized by even a moderate stress-assisted ionic flux. In other words, if additional destabilizing factors exist, for example, mass-transport limitation in polymer electrolytes, they can cause irregular growth and mechanical bias to reaction kinetics may not be sufficient to regularize such a tendency. In fact, the dominant cause of irregular growth in polymer electrolytes is the local ionic depletion[16, 33, 46]. On the other hand, stiff electrolytes provide sufficient stress levels that could stabilize irregular growth, however, they are limited by molar volume mismatch. Explained differently, stiff electrolytes exhibit spontaneous drive for localized growth and can be stabilized given sufficiently strong mechanical – transport interplay. Thus, regime I implies thermodynamically unstable but kinetically stable deposition (in this viewpoint[70], 'thermodynamic' refers to free energy difference and spontaneity, while 'kinetic' refers to transient interactions). On the other hand, soft electrolytes, given the smaller stresses do not exhibit a strong preference for irregular growth. Thus, they represent a condition of (near) thermodynamic stability and kinetic stability. The electrodeposition in liquid electrolytes does not exhibit any spontaneity for localized growth, and the concentration gradients generated during current passage leads to unstable growth. Thus, electrodeposition in liquid electrolytes is thermodynamically stable but kinetically unstable.

Notice that for soft electrolytes, smaller mechanical stresses do not cause considerable asymmetry in electrodeposition reaction. However, these stresses could still contribute to ionic transport as a stabilizing influence. This leads to a particularly interesting possibility in polymer electrolytes that exhibit irregular growth largely due to ionic depletion at the depositing electrode. In such electrolytes, stress-driven ionic conduction could be leveraged (via tuning stress conductivity, κ_σ) to counter the diffusion limitation. Such mechanics – transport interplay could even be advantageous for future solid electrolytes.

The electrodeposition stability with material complexities such as interphase and grain boundaries is also modified by stiffness effects discussed in Figure 4. An efficient interphase material has high stiffness as well as matched molar volumes. On the other hand, grain boundaries can improve stability if they fall in regime I, for example, if the stiffness of grain boundaries is 50% that of grains (as predicted from MD calculations[71]) for LLZO, electrodeposition is expected to become more stable. Thence, the observed intergranular growth in LLZO[23] probably results from increased cationic molar volume as argued in Figure 3(b). Alternatively, if grain boundaries are softer such that they lie in regime II, unstable growth is expected to originate predominantly in grain boundaries.

Dynamic Growth

Preceding discussion characterizes static stability where reaction distribution is assessed based on a preset deposition profile. Such an interpretation comments on intrinsic

stabilizing tendency of different material interactions. When lithium grows continuously, new lithium deposits every time instant, which changes the stress field and ionic currents to cause further deposition. The deposition profile changes continuously in response to the new fields. As lithium grows, the solid electrolyte as a whole also shifts, which indirectly affects deformations.

Critical current density[23, 26] is often used as an indicator of electrodeposition stability. It is measured based on continuous growth that causes extended irregular deposition. Given the difference in static stability analyzed here and dynamic growth during experimental measurements, the propensity for irregular growth is quantified in terms of critical distortions. The two are equivalent and scale similarly. An electrolyte with a higher critical distortion is expected to exhibit a larger critical current density.

Since the static stability inferences assess the intrinsic tendency of material interactions, it equally translates to the stability of a dynamic growth under different operating conditions (note that critical current density measurements are carried out at constant current). For example, Porz *et al.*[35], characterize stability via linearly increasing deposition rate, where the departure of applied voltage from a linear rise marks the onset of unstable growth. In such an instant, critical distortion relates to the onset time for departure from a linear rise.

Plastic Deformations

In terms of mechanical properties, lithium is a soft metal[18, 71, 78-79], i.e., it can easily undergo plastic deformation. Often yield strain, ε_Y, is specified to demarcate the onset of plasticity. For strains smaller than the yield strain, stresses scale linearly with strains. Beyond yield strain, large geometrical changes can take place with marginal changes in stress. Given the high stiffness of inorganic electrolytes (regime I), even a small irregular deposition leads to large enough stresses to cause plastic deformation in lithium[16]. Plastic deformation causes large volumetric changes to accommodate new growth. Correspondingly, hydrostatic stress profile in lithium is expected to contain fairly uniform stresses (approximately equal to yield stress, σ_Y) at the locations of stress extremes, i.e., peaks and valleys, and small variations in between (compare against Figure 2(c)). The mechanical overpotential, η_σ, profile adopts an equivalent shape which in turn translates into reaction distribution. Thus, unlike elastic deformations where profiles of new deposition, stresses (Figure 2(c)) and current distribution (Figure 2(f)unstable) are qualitatively similar for an unstable growth, stress and current profiles can differ which leads to more rapid changes in growth front to accommodate large plastic deformations. Further complications arise due to strain hardening and viscoplasticity effects in lithium[72].

Very soft electrolytes (regime III) can undergo plastic deformations themselves to accommodate fresh deposition. Given the weak coupling between stresses and kinetics, the

current distribution is not expected to change much. Consequently, the electrodepositing interface will evolve largely in response to ionic transport.

These plasticity effects largely manifest during dynamic growth in regimes I and III.

Origins of Wettability

The non-conformity of solid-solid interface essentially relates to a physical mismatch (characterized by surface roughness) and a material discontinuity (sudden compositional change)[70]. Presence of asperities at the solid surface reduces the effective contact area and causes localized contact at the active interface. Such spots could lead to localized deposition and in turn, irregular growth. One remedy is to increase external pressure[18] to ensure a more thorough match. Typically, cells are fabricated in a compressed state to ensure good contact at different interfaces. However, the external pressure levels cannot be tuned over a wide range. A more thoughtful approach is to use conformal materials, e.g., interlayer, to fill the asperities and affect a congruent interface[29, 67]. They effectively improve the contact, but also alter reaction landscape. In addition to the conventional interfacing requirement of conducting flux (heat flow[64] or electric current), herein electrodeposition reaction is to be facilitated as well. Accordingly, description of the desirable qualities of a suitable interlayer is more involved.

Any material interface is characterized by surface energy. Surface energy (equivalently surface tension) contributes to mechanical forces[44, 70]. Since stresses are central to solid electrolyte operation, the role of surface energy should be examined. A low surface energy interface allows more intimate contact between the two adjoining materials. For example, contact angle (wetting) measurements of molten lithium – solid electrolyte indicate that the presence of surface phases, e.g., Li_2CO_3 and LiOH, is detrimental to the interfacial contact[29, 67, 73-74].

Improved wetting could result from better physical contact, i.e., smaller roughness (physical wettability) and/or a low energy interface (chemical wettability). But their contributions to electrodeposition are very different given the underlying differences in material interactions. A force balance at the interface shows $\sigma_{Li} \cdot \hat{n} + \gamma\varkappa = \sigma_e \cdot \hat{n}$. Scaling analysis further reveals that $\sigma \sim \mathcal{O}\left(G\xi/\lambda\right)$ and $\gamma\varkappa \sim \mathcal{O}\left(\gamma\xi/\lambda^2\right)$. Equivalently, surface energy contributes to electrodeposition dynamics only when $G \sim \mathcal{O}\left(\gamma/\lambda\right)$, i.e., for kPa – MPa stiffnesses. Very soft polymer electrolytes and liquid electrolytes fall in this category, and a surface tension dependent regime should emerge in Figure 4(b). Such an interpretation (scaling analysis) is consistent with interfacial energy effects observed in very soft substrates[75-76]. Since inorganic solid electrolytes (even stiff polymers) are comparatively stiffer, surface tension does not contribute to continuous growth (nucleation is always a surface energy dependent phenomenon).

As compared to direct contact between lithium and solid electrolyte, an interface material (e.g., interlayer or surface film) exhibits a different cationic volume. Impedance analysis (section S5) reveals that the charge transfer resistance, R_{ct}, relates to (interfacial) partial molar volume as per the expression:

$$R_{\text{ct}} = \frac{RT}{F} \cdot \frac{1}{i_0 {}^{a}/_{a_0}} exp\left(\frac{p\Omega_{Li}}{2RT}\left({}^{\Omega_{Li^+}}/_{\Omega_{Li}} - 1\right)\right) \tag{3}$$

where the exponential term describes the molar volume mismatch, and the area ratio, ${}^{a}/_{a_0}$, in the denominator accounts for imperfect physical contact. Both the terms scale with pressure, however, the qualitative nature of the pressure variation differs. When physical wetting is a dominant, contact resistance decreases with pressure. On the other hand, when molar volume mismatch is dominant, contact resistance increases with pressure. Thus, improved electrodeposition stability in interfacial modifications fundamentally arises from physical wetting and molar volume mismatch, and not due to surface energy based chemical wetting. For consistency of terminology, molar volume mismatch should be termed 'electrochemical wetting' (perfect electrochemical wetting would imply matched molar volumes, $\Omega_{Li^+} = \Omega_{Li}$). Note that in order to interpret an experimental impedance data using expression (3), contact resistance values should be fit against pressure. Given qualitatively disparate pressure dependence of physical and electrochemical wetting effects, relevant properties such as exchange current density, i_0, and cationic molar volume, Ω_{Li^+}, would be obtained as solutions of regression analysis. Exchange current density, i_0, can be verified independently through cyclic voltammetry or other equivalent techniques (an appropriate asymmetric form of kinetic expression should be used for inferences). We hope that such an indirect estimation of the partial molar volume provides the much needed information.

Conclusions

Lithium electrodeposition in solid electrolytes has been a scientific mystery given the incomplete understanding of underlying material interactions. We analyze the electrochemical growth using non-equilibrium thermodynamics to underpin the coupling among stress and ionic fields. Molar volumes characterize the mechanical energy of reacting species. Consequently, when stressed, a high molar volume species (here cation) locally converts to a lower molar volume species (here metal) to reduce energy. Such spontaneity biases the reaction kinetics. Stresses close to a solid – solid interface are correlated, in turn, spontaneity (i.e., drive for irregular growth) scales with molar volume mismatch.

Stress distribution in solid electrolytes causes stress-driven ionic flux from compressive to tensile locations. Localized deposition generates compressive stresses which could divert ionic flux away and in turn provide a stabilizing influence. For electrolytes exhibiting diffusion-limited unstable electrodeposition, such stress-driven ionic transport can be tuned to regularize growth.

Interfacial stresses scale with electrolyte stiffness. Stiffer electrolytes result in a greater spontaneity for localized deposition. On the other hand, softer electrolytes exhibit marginal reaction asymmetry due to much smaller stresses. For electrolytes with stiffness comparable to lithium $(2G_{Li} \gtrsim G_e \gtrsim {}^{G_{Li}}/_{2})$, stress fields are very similar and consequently, even a small mismatch of molar volumes favor irregular growth.

The effectiveness of material modifications such as interphase and interlayers relates to their stiffness as well as cationic molar volumes. Lithium can selectively deposit along grain boundaries either due to larger cationic molar volume or lithium like stiffness.

An effective solid electrolyte is not just stiffer than lithium but also exhibits comparable cationic molar volume (ideally same as lithium). Matched molar volumes ensure minimized spontaneity for irregular growth. Furthermore, enhancing stress-driven conduction in the electrolyte can divert ionic flux away from compressed locations and facilitate conditional stability.

Mechanical and ionic fields vary fairly close to the electrochemical interface with a lengthscale comparable to average separation between nucleation sites. As a result, reduction in electrolyte thickness from present-day solid electrolyte thickness $(\sim 500\ \mu\mathrm{m})$ to present-day liquid electrolyte thickness $(\sim 20\ \mu\mathrm{m})$ is unlikely ameliorate the mechanically induced irregular growth. The current analysis is equally applicable to other metallic anodes, e.g., sodium, magnesium, aluminum, with appropriate solid electrolyte (stiffness regimes should be interpreted in terms of respective metals).

Supporting Information includes

S1. A Critique on Mechanistic Interpretation of Solid Electrolyte Failure (Table S1)
S2. Theoretical Description of Electrodeposition Stability with Solid Electrolytes (Figure S1, S2; Table S2, S3)
S3. Electrodeposition Kinetics at the Solid – Solid Interface (Figure S3)
S4. Physical Interpretation of (Partial) Molar Volume
S5. Charge Transfer Resistance of a Stressed Electrochemical Interface (Figure S4)
S6. Non-equilibrium Charge Transport in a Solid Electrolyte
S7. Unusual Lithium Growth in Polymer Electrolyte (Figure S5)

Acknowledgments

Financial support in part from National Science Foundation (grant no. 1805656) and Purdue University is gratefully acknowledged.

References

(1) Mistry, A. N.; Smith, K.;Mukherjee, P. P. Secondary-Phase Stochastics in Lithium-Ion Battery Electrodes. *ACS Appl. Mater. Interfaces* **2018**, *10*, 6317-6326.
(2) Mistry, A. N.;Mukherjee, P. P. "Shuttle" in Polysulfide Shuttle: Friend or Foe? *J. Phys. Chem. C* **2018**, *122*, 23845-23851.
(3) Mistry, A. N.; Cano-Banda, F.; Law, D.; Hernandez-Guerrero, A.;Mukherjee, P. P. Non-Equilibrium Thermodynamics in Electrochemical Complexation of Li–Oxygen Porous Electrodes. *J. Mater. Chem. A* **2019**, *7*, 8882-8888.

(4) Mistry, A.; Fear, C.; Carter, R.; Love, C. T.;Mukherjee, P. P. Electrolyte Confinement Alters Lithium Electrodeposition. *ACS Energy Lett.* **2019**, *4*, 156-162.
(5) Bai, P.; Li, J.; Brushett, F. R.;Bazant, M. Z. Transition of Lithium Growth Mechanisms in Liquid Electrolytes. *Energy Environ. Sci.* **2016**, *9*, 3221-3229.
(6) Bai, P.; Guo, J.; Wang, M.; Kushima, A.; Su, L.; Li, J.; Brushett, F. R.;Bazant, M. Z. Interactions between Lithium Growths and Nanoporous Ceramic Separators. *Joule* **2018**, *2*, 2434-2449.
(7) Chen, K.-H.; Wood, K. N.; Kazyak, E.; LePage, W. S.; Davis, A. L.; Sanchez, A. J.;Dasgupta, N. P. Dead Lithium: Mass Transport Effects on Voltage, Capacity, and Failure of Lithium Metal Anodes. *J. Mater. Chem. A* **2017**, *5*, 11671-11681.
(8) Wood, K. N.; Kazyak, E.; Chadwick, A. F.; Chen, K.-H.; Zhang, J.-G.; Thornton, K.;Dasgupta, N. P. Dendrites and Pits: Untangling the Complex Behavior of Lithium Metal Anodes through Operando Video Microscopy. *ACS Cent. Sci.* **2016**, *2*, 790-801.
(9) Bieker, G.; Winter, M.;Bieker, P. Electrochemical in Situ Investigations of Sei and Dendrite Formation on the Lithium Metal Anode. *Phys. Chem. Chem. Phys.* **2015**, *17*, 8670-8679.
(10) Wang, T.; Villegas Salvatierra, R.; Jalilov, A. S.; Tian, J.;Tour, J. M. Ultrafast Charging High Capacity Asphalt–Lithium Metal Batteries. *ACS Nano* **2017**, *11*, 10761-10767.
(11) Davidson, R.; Verma, A.; Santos, D.; Hao, F.; Fincher, C.; Xiang, S.; Van Buskirk, J.; Xie, K.; Pharr, M.; Mukherjee, P. P.;Banerjee, S. Formation of Magnesium Dendrites During Electrodeposition. *ACS Energy Lett.* **2019**, *4*, 375-376.
(12) Wei, S.; Cheng, Z.; Nath, P.; Tikekar, M. D.; Li, G.;Archer, L. A. Stabilizing Electrochemical Interfaces in Viscoelastic Liquid Electrolytes. *Sci. Adv.* **2018**, *4*, eaao6243.
(13) Choudhury, S.; Vu, D.; Warren, A.; Tikekar, M. D.; Tu, Z.;Archer, L. A. Confining Electrodeposition of Metals in Structured Electrolytes. *Proceedings of the National Academy of Sciences* **2018**, *115*, 6620-6625.
(14) Monroe, C.;Newman, J. The Effect of Interfacial Deformation on Electrodeposition Kinetics. *J. Electrochem. Soc.* **2004**, *151*, A880-A886.
(15) Monroe, C.;Newman, J. The Impact of Elastic Deformation on Deposition Kinetics at Lithium/Polymer Interfaces. *J. Electrochem. Soc.* **2005**, *152*, A396-A404.
(16) Barai, P.; Higa, K.;Srinivasan, V. Lithium Dendrite Growth Mechanisms in Polymer Electrolytes and Prevention Strategies. *Phys. Chem. Chem. Phys.* **2017**, *19*, 20493-20505.
(17) Barai, P.; Higa, K.;Srinivasan, V. Effect of Initial State of Lithium on the Propensity for Dendrite Formation: A Theoretical Study. *J. Electrochem. Soc.* **2017**, *164*, A180-A189.
(18) Barai, P.; Higa, K.;Srinivasan, V. Impact of External Pressure and Electrolyte Transport Properties on Lithium Dendrite Growth. *J. Electrochem. Soc.* **2018**, *165*, A2654-A2666.
(19) Ahmad, Z.;Viswanathan, V. Stability of Electrodeposition at Solid-Solid Interfaces and Implications for Metal Anodes. *Phys. Rev. Lett.* **2017**, *119*, 056003.
(20) Ahmad, Z.;Viswanathan, V. Role of Anisotropy in Determining Stability of Electrodeposition at Solid-Solid Interfaces. *Physical Review Materials* **2017**, *1*, 055403.
(21) Ahmad, Z.; Xie, T.; Maheshwari, C.; Grossman, J. C.;Viswanathan, V. Machine Learning Enabled Computational Screening of Inorganic Solid Electrolytes for Suppression of Dendrite Formation in Lithium Metal Anodes. *ACS Cent. Sci.* **2018**, *4*, 996-1006.
(22) Schnell, J.; Tietz, F.; Singer, C.; Hofer, A.; Billot, N.;Reinhart, G. Prospects of Production Technologies and Manufacturing Costs of Oxide-Based All-Solid-State Lithium Batteries. *Energy Environ. Sci.* **2019**.
(23) Cheng, E. J.; Sharafi, A.;Sakamoto, J. Intergranular Li Metal Propagation through Polycrystalline Li6. 25al0. 25la3zr2o12 Ceramic Electrolyte. *Electrochim. Acta* **2017**, *223*, 85-91.
(24) Garcia-Mendez, R.; Mizuno, F.; Zhang, R.; Arthur, T. S.;Sakamoto, J. Effect of Processing Conditions of 75li2s-25p2s5 Solid Electrolyte on Its Dc Electrochemical Behavior. *Electrochim. Acta* **2017**, *237*, 144-151.
(25) Smith, S.; Thompson, T.; Sakamoto, J.; Allen, J. L.; Baker, D. R.;Wolfenstine, J. Electrical, Mechanical and Chemical Behavior of Li1. 2zr1. 9sr0. 1 (Po4) 3. *Solid State Ionics* **2017**, *300*, 38-45.
(26) Taylor, N. J.; Stangeland-Molo, S.; Haslam, C. G.; Sharafi, A.; Thompson, T.; Wang, M.; Garcia-Mendez, R.;Sakamoto, J. Demonstration of High Current Densities and Extended Cycling in the Garnet Li 7 La 3 Zr 2 O 12 Solid Electrolyte. *J. Power Sources* **2018**, *396*, 314-318.
(27) Han, X.; Gong, Y.; Fu, K. K.; He, X.; Hitz, G. T.; Dai, J.; Pearse, A.; Liu, B.; Wang, H.;Rubloff, G. Negating Interfacial Impedance in Garnet-Based Solid-State Li Metal Batteries. *Nat. Mater.* **2017**, *16*, 572.
(28) Liu, B.; Gong, Y.; Fu, K.; Han, X.; Yao, Y.; Pastel, G.; Yang, C.; Xie, H.; Wachsman, E. D.;Hu, L. Garnet Solid Electrolyte Protected Li-Metal Batteries. *ACS Appl. Mater. Interfaces* **2017**, *9*, 18809-18815.
(29) Luo, W.; Gong, Y.; Zhu, Y.; Fu, K. K.; Dai, J.; Lacey, S. D.; Wang, C.; Liu, B.; Han, X.;Mo, Y. Transition from Superlithiophobicity to Superlithiophilicity of Garnet Solid-State Electrolyte. *J. Am. Chem. Soc.* **2016**, *138*, 12258-12262.
(30) Harry, K. J.; Hallinan, D. T.; Parkinson, D. Y.; MacDowell, A. A.;Balsara, N. P. Detection of Subsurface Structures Underneath Dendrites Formed on Cycled Lithium Metal Electrodes. *Nat. Mater.* **2014**, *13*, 69.

(31) Harry, K. J.; Higa, K.; Srinivasan, V.;Balsara, N. P. Influence of Electrolyte Modulus on the Local Current Density at a Dendrite Tip on a Lithium Metal Electrode. *J. Electrochem. Soc.* **2016**, *163*, A2216-A2224.
(32) Maslyn, J. A.; Loo, W. S.; McEntush, K. D.; Oh, H. J.; Harry, K. J.; Parkinson, D. Y.;Balsara, N. P. Growth of Lithium Dendrites and Globules through a Solid Block Copolymer Electrolyte as a Function of Current Density. *J. Phys. Chem. C* **2018**, *122*, 26797-26804.
(33) Pesko, D. M.; Feng, Z.; Sawhney, S.; Newman, J.; Srinivasan, V.;Balsara, N. P. Comparing Cycling Characteristics of Symmetric Lithium-Polymer-Lithium Cells with Theoretical Predictions. *J. Electrochem. Soc.* **2018**, *165*, A3186-A3194.
(34) Swamy, T.; Park, R.; Sheldon, B. W.; Rettenwander, D.; Porz, L.; Berendts, S.; Uecker, R.; Carter, W. C.;Chiang, Y.-M. Lithium Metal Penetration Induced by Electrodeposition through Solid Electrolytes: Example in Single-Crystal Li6la3zrtao12 Garnet. *J. Electrochem. Soc.* **2018**, *165*, A3648-A3655.
(35) Porz, L.; Swamy, T.; Sheldon, B. W.; Rettenwander, D.; Frömling, T.; Thaman, H. L.; Berendts, S.; Uecker, R.; Carter, W. C.;Chiang, Y. M. Mechanism of Lithium Metal Penetration through Inorganic Solid Electrolytes. *Adv. Energy Mater.* **2017**, *7*, 1701003.
(36) Li, Y.; Zhou, W.; Chen, X.; Lü, X.; Cui, Z.; Xin, S.; Xue, L.; Jia, Q.;Goodenough, J. B. Mastering the Interface for Advanced All-Solid-State Lithium Rechargeable Batteries. *Proceedings of the National Academy of Sciences* **2016**, *113*, 13313-13317.
(37) Wu, B.; Wang, S.; Lochala, J.; Desrochers, D.; Liu, B.; Zhang, W.; Yang, J.;Xiao, J. The Role of the Solid Electrolyte Interphase Layer in Preventing Li Dendrite Growth in Solid-State Batteries. *Energy Environ. Sci.* **2018**, *11*, 1803-1810.
(38) Sun, F.; Dong, K.; Osenberg, M.; Hilger, A.; Risse, S.; Lu, Y.; Kamm, P. H.; Klaus, M.; Markötter, H.; García-Moreno, F.; Arlt, T.;Manke, I. Visualizing the Morphological and Compositional Evolution of the Interface of Inli-Anode|Thio-Lision Electrolyte in an All-Solid-State Li–S Cell by in Operando Synchrotron X-Ray Tomography and Energy Dispersive Diffraction. *J. Mater. Chem. A* **2018**, *6*, 22489-22496.
(39) Han, F.; Westover, A. S.; Yue, J.; Fan, X.; Wang, F.; Chi, M.; Leonard, D. N.; Dudney, N. J.; Wang, H.;Wang, C. High Electronic Conductivity as the Origin of Lithium Dendrite Formation within Solid Electrolytes. *Nat. Energy* **2019**, 1.
(40) Lewis, J. A.; Cortes, F. J. Q.; Boebinger, M. G.; Tippens, J.; Marchese, T. S.; Kondekar, N. P.; Liu, X.; Chi, M.;McDowell, M. T. Interphase Morphology between a Solid-State Electrolyte and Lithium Controls Cell Failure. *ACS Energy Lett.* **2019**.
(41) Drazin, P. G.;Reid, W. H. *Hydrodynamic Stability*; Cambridge university press, 2004.
(42) Chandrasekhar, S. *Hydrodynamic and Hydromagnetic Stability*; Courier Corporation, 2013.
(43) Mullins, W. W.;Sekerka, R. F. Stability of a Planar Interface During Solidification of a Dilute Binary Alloy. *J. Appl. Phys.* **1964**, *35*, 444-451.
(44) Balluffi, R. W.; Allen, S.;Carter, W. C. *Kinetics of Materials*; John Wiley & Sons, 2005.
(45) Newman, J.;Thomas-Alyea, K. E. *Electrochemical Systems*; John Wiley & Sons: New Jersey, 2012.
(46) Rosso, M.; Brissot, C.; Teyssot, A.; Dollé, M.; Sannier, L.; Tarascon, J.-M.; Bouchet, R.;Lascaud, S. Dendrite Short-Circuit and Fuse Effect on Li/Polymer/Li Cells. *Electrochim. Acta* **2006**, *51*, 5334-5340.
(47) Liu, X.; Chen, Y.; Hood, Z. D.; Ma, C.; Yu, S.; Sharafi, A.; Wang, H.; An, K.; Sakamoto, J.; Siegel, D. J.; Cheng, Y.; Jalarvo, N. H.;Chi, M. Elucidating the Mobility of H+ and Li+ Ions in (Li6.25−Xhxal0.25)La3zr2o12via Correlative Neutron and Electron Spectroscopy. *Energy Environ. Sci.* **2019**, *12*, 945-951.
(48) Posch, P.; Lunghammer, S.; Berendts, S.; Ganschow, S.; Redhammer, G. J.; Wilkening, A.; Lerch, M.; Gadermaier, B.; Rettenwander, D.;Wilkening, H. M. R. Ion Dynamics in Al-Stabilized Li7la3zr2o12 Single Crystals–Macroscopic Transport and the Elementary Steps of Ion Hopping. *Energy Storage Materials* **2019**.
(49) Barai, P.; Higa, K.; Ngo, A. T.; Curtiss, L. A.;Srinivasan, V. Mechanical Stress Induced Current Focusing and Fracture in Grain Boundaries. *J. Electrochem. Soc.* **2019**, *166*, A1752-A1762.
(50) Yu, S.;Siegel, D. J. Grain Boundary Contributions to Li-Ion Transport in the Solid Electrolyte Li7la3zr2o12 (Llzo). *Chem. Mater.* **2017**, *29*, 9639-9647.
(51) Li, J. C.-M. Physical Chemistry of Some Microstructural Phenomena. *Metall. Trans. A* **1978**, *9*, 1353-1380.
(52) Guggenheim, E. A. Thermodynamics-an Advanced Treatment for Chemists and Physicists. *Amsterdam, North-Holland, 1985, 414 p.* **1985**.
(53) De Groot, S. R.;Mazur, P. *Non-Equilibrium Thermodynamics*; Courier Corporation, 2013.
(54) Nagao, M.; Hayashi, A.;Tatsumisago, M. High-Capacity Li2s–Nanocarbon Composite Electrode for All-Solid-State Rechargeable Lithium Batteries. *J. Mater. Chem.* **2012**, *22*, 10015-10020.
(55) Timoshenko, S. P.;Gere, J. M. *Theory of Elastic Stability*; Courier Corporation, 2009.
(56) Malvern, L. E. *Introduction to the Mechanics of a Continuous Medium*, 1969.
(57) Bower, A. F. *Applied Mechanics of Solids*; CRC press, 2009.
(58) Valøen, L. O.;Reimers, J. N. Transport Properties of Lipf6-Based Li-Ion Battery Electrolytes. *J. Electrochem. Soc.* **2005**, *152*, A882-A891.

(59) Larson, J. M.; Gillette, E.; Burson, K.; Wang, Y.; Lee, S. B.;Reutt-Robey, J. E. Pascalammetry with Operando Microbattery Probes: Sensing High Stress in Solid-State Batteries. *Sci. Adv.* **2018**, *4*, eaas8927.
(60) McMeeking, R. M.; Ganser, M.; Klinsmann, M.;Hildebrand, F. E. Metal Electrode Surfaces Can Roughen Despite the Constraint of a Stiff Electrolyte. *J. Electrochem. Soc.* **2019**, *166*, A984-A995.
(61) Khoo, E.; Zhao, H.;Bazant, M. Z. Linear Stability Analysis of Transient Electrodeposition in Charged Porous Media: Suppression of Dendritic Growth by Surface Conduction. *J. Electrochem. Soc.* **2019**, *166*, A2280-A2299.
(62) Krauskopf, T.; Dippel, R.; Hartmann, H.; Peppler, K.; Mogwitz, B.; Richter, F. H.; Zeier, W. G.;Janek, J. Lithium-Metal Growth Kinetics on Llzo Garnet-Type Solid Electrolytes. *Joule* **2019**.
(63) Porter, D. A.; Easterling, K. E.;Sherif, M. *Phase Transformations in Metals and Alloys, (Revised Reprint)*; CRC press, 2009.
(64) Chung, D. D. L. Thermal Interface Materials. *J. Mater. Eng. Perform.* **2001**, *10*, 56-59.
(65) Liu, B.; Fu, K.; Gong, Y.; Yang, C.; Yao, Y.; Wang, Y.; Wang, C.; Kuang, Y.; Pastel, G.;Xie, H. Rapid Thermal Annealing of Cathode-Garnet Interface toward High-Temperature Solid State Batteries. *Nano Lett.* **2017**, *17*, 4917-4923.
(66) Luo, W.; Gong, Y.; Zhu, Y.; Li, Y.; Yao, Y.; Zhang, Y.; Fu, K.; Pastel, G.; Lin, C. F.;Mo, Y. Reducing Interfacial Resistance between Garnet-Structured Solid-State Electrolyte and Li-Metal Anode by a Germanium Layer. *Adv. Mater.* **2017**, *29*, 1606042.
(67) Fu, K. K.; Gong, Y.; Liu, B.; Zhu, Y.; Xu, S.; Yao, Y.; Luo, W.; Wang, C.; Lacey, S. D.;Dai, J. Toward Garnet Electrolyte–Based Li Metal Batteries: An Ultrathin, Highly Effective, Artificial Solid-State Electrolyte/Metallic Li Interface. *Sci. Adv.* **2017**, *3*, e1601659.
(68) Zhao, K.; Pharr, M.; Wan, Q.; Wang, W. L.; Kaxiras, E.; Vlassak, J. J.;Suo, Z. Concurrent Reaction and Plasticity During Initial Lithiation of Crystalline Silicon in Lithium-Ion Batteries. *J. Electrochem. Soc.* **2012**, *159*, A238-A243.
(69) Pharr, M.; Choi, Y. S.; Lee, D.; Oh, K. H.;Vlassak, J. J. Measurements of Stress and Fracture in Germanium Electrodes of Lithium-Ion Batteries During Electrochemical Lithiation and Delithiation. *J. Power Sources* **2016**, *304*, 164-169.
(70) Israelachvili, J. N. *Intermolecular and Surface Forces*; Academic press: New York, 2011.
(71) Yu, S.;Siegel, D. J. Grain Boundary Softening: A Potential Mechanism for Lithium Metal Penetration through Stiff Solid Electrolytes. *ACS Appl. Mater. Interfaces* **2018**, *10*, 38151-38158.
(72) LePage, W. S.; Chen, Y.; Kazyak, E.; Chen, K.-H.; Sanchez, A. J.; Poli, A.; Arruda, E. M.; Thouless, M. D.;Dasgupta, N. P. Lithium Mechanics: Roles of Strain Rate and Temperature and Implications for Lithium Metal Batteries. *J. Electrochem. Soc.* **2019**, *166*, A89-A97.
(73) Sharafi, A.; Kazyak, E.; Davis, A. L.; Yu, S.; Thompson, T.; Siegel, D. J.; Dasgupta, N. P.;Sakamoto, J. Surface Chemistry Mechanism of Ultra-Low Interfacial Resistance in the Solid-State Electrolyte Li7la3zr2o12. *Chem. Mater.* **2017**, *29*, 7961-7968.
(74) Wang, J.; Wang, H.; Xie, J.; Yang, A.; Pei, A.; Wu, C.-L.; Shi, F.; Liu, Y.; Lin, D.;Gong, Y. Fundamental Study on the Wetting Property of Liquid Lithium. *Energy Storage Materials* **2018**, *14*, 345-350.
(75) Andreotti, B.; Bäumchen, O.; Boulogne, F.; Daniels, K. E.; Dufresne, E. R.; Perrin, H.; Salez, T.; Snoeijer, J. H.;Style, R. W. Solid Capillarity: When and How Does Surface Tension Deform Soft Solids? *Soft Matter* **2016**, *12*, 2993-2996.
(76) Lubbers, L. A.; Weijs, J. H.; Botto, L.; Das, S.; Andreotti, B.;Snoeijer, J. H. Drops on Soft Solids: Free Energy and Double Transition of Contact Angles. *J. Fluid Mech.* **2014**, *747*.

Supporting Information

Molar Volume Mismatch: a Malefactor for Irregular Metallic Electrodeposition in Solid Electrolytes

Aashutosh N. Mistry[1†] and Partha P. Mukherjee[2*]

School of Mechanical Engineering, Purdue University, West Lafayette, IN 47907, United States

Electrodeposition of lithium at the interface with a solid (inorganic) electrolyte differs from the more commonly studied plating scenarios in contact with liquid[1-4] or polymer electrolytes[5-9]. The reaction kinetics at the electrified interface as well as the ionic transport in these solid electrolytes disagree with their conventional counterparts given the dissimilarities in the interfacial as well as bulk structures. The following discussion starts by surveying the mechanistic beliefs on electrodeposition, especially at the interface with a solid (inorganic) electrolyte, to pose the conflicting thoughts and unanswered questions. Subsequently, the problem is described in mathematical terms with appropriate physical constraints. The reaction and transport interactions in this system have been reformulated based on non-equilibrium thermodynamics[10]. Discussions are grouped into the following sections:

S1. A Critique on Mechanistic Interpretation of Solid Electrolyte Failure

The usefulness of metallic electrodes (e.g., lithium) lies in maintaining a uniform electrodeposition front at large currents. Given the thermal fluctuations and associated stochasticity, microscopically, electrodeposition is composed of discrete nucleation and growth events[1, 11-13]. Accounting for such microscopic irregularity, a stable electrodeposition

* Email: pmukherjee@purdue.edu
† present address: Argonne National Laboratory, United States
[1] ORCID: 0000 – 0002 – 4359 – 4975
[2] ORCID: 0000 – 0001 – 7900 – 7261

front is the one that does not amplify the coarseness of the metal – electrolyte interface with continued deposition.

Theoretical studies of Monroe and Newman[3, 5, 14] argued if mechanically stiff electrolytes (i.e., solids) are used, uneven stress-field resulting from irregular deposition provides a balancing influence. However, sufficiently stiff solid electrolytes are still found to give rise to highly irregular electrodeposition scenario[15-16]. Several mechanisms (Table S1) have been proposed to account for this anomalous response, but, none so far accounts for the different observations which are found to be characteristic of electrodeposition with the (inorganic) solid electrolytes (Eq. (S1)).

Characteristics of lithium electrodeposition with (inorganic) solid electrolytes:

- Irregular lithium electrodeposition even with stiff solid electrolytes[15-16]
- In polycrystalline electrolytes, lithium deposits along the grain boundaries[15]
- Single crystal, as well as amorphous electrolytes, also exhibit irregular electrodeposition[16]
- Interphases either promote[17] or demote[18-19] nonuniformity
- Interlayers can be helpful in controlling the uniformity of electrodeposition[20-21]

(S1)

Given the uncertainty of mechanistic origins of electrodeposition instability in the inorganic solid electrolytes, the electrochemical interactions of solid ion conductors are poorly understood.

Table S1. Examining previously proposed mechanisms: A summary of representative literature on unstable electrodeposition in solid electrolytes with an emphasis on mechanistic interpretation. The studies are identified by the corresponding author in alphabetical order.

Nitash Balsara[6-7, 22-23]	
	Tomographic and electrochemical investigations of electrodeposition with soft polymer electrolytes $\left(G_e/G_{Li} \sim 10^{-3} - 10^{-4}\right)$.
Yet-Ming Chiang[16, 24-26]	
	Electrodeposition experiments on amorphous, polycrystalline and single-crystal inorganic electrolytes; Pre-existing cracks are recognized as the preferential lithium filling sites and sustained fracture given stress concentration at the lithium tip.
John Goodenough[18]	
	A new solid electrolyte ($LiZr_2(PO)_4$) is studied which reacts with Li to form stable interphase that simultaneously prohibits further reaction (i.e., thickness does not change), ensures conformal contact and conducts Li^+.

Matthew McDowell[17]	
	Li and electrolyte (here LAGP) react to form interphase that is amorphous and experiences fracture; The irregularity of the interphase could offer shorter lithium transport pathways, which further becomes locations for increased ionic flux and reduced stability.
Robert McMeeking[27-28]	
	A revised kinetic description, i.e., Butler-Volmer, is formulated using solid stresses; Linear stability analysis around a stress-free state recognizes a stiffness-independent unstable growth for large wavelength perturbations.
Charles Monroe[29]	
	Argues that high stresses make lithium deposition inside electrolyte at the grain boundaries energetically favorable.
John Newman[3, 5, 14]	
	Electrochemical kinetics is modified to account for stress imbalance at the interface; Electrode – electrolyte interface is perturbed to quantify the condition for unstable deposition; Stable deposition for $G_e > 2G_{Li}$.
Jeff Sakamoto[15, 30-34]	
	Experiments with different inorganic solid electrolytes to assess the influence of processing and operating conditions; Unwanted chemical and/or electrochemical reactions are detected at the Li – electrolyte interface; Nonuniform Li deposition is found to preferentially take place along the grain boundaries in a polycrystalline LLZO.
Donald Siegel[35-39]	
	Grain boundary diffusion and stiffness are estimated to ascertain their role in intergranular Li deposition; Surface layers of Li_2CO_3 and LiOH are found to increase the interface energy of Li – electrolyte contact, which negatively affects stability.
Venkat Srinivasan[40-43]	
	Extends the Newman analysis for i. pre-stressed interfaces ii. nonplanar unperturbed interfaces iii. electrolyte transport iv. plastic deformation of lithium v. grain boundary mechanics and transport
Venkat Viswanathan[44-46]	
	Extends the Newman analysis for anisotropic mechanical properties arising from different crystal orientations.

Eric Wachsman[20-21, 47-53]	
	Various interlayers (Si, Al_2O_3, Ge, Al, Mg, and gel-electrolyte) are shown to reduce interfacial resistance and promote more stable deposition.
Chunsheng Wang[54]	
	Neutron depth profiling of two inorganic solid electrolytes (LLZO and LPS) reveal some lithium deposition in the bulk; Electronic current has been argued as the cause for non-interfacial deposition.

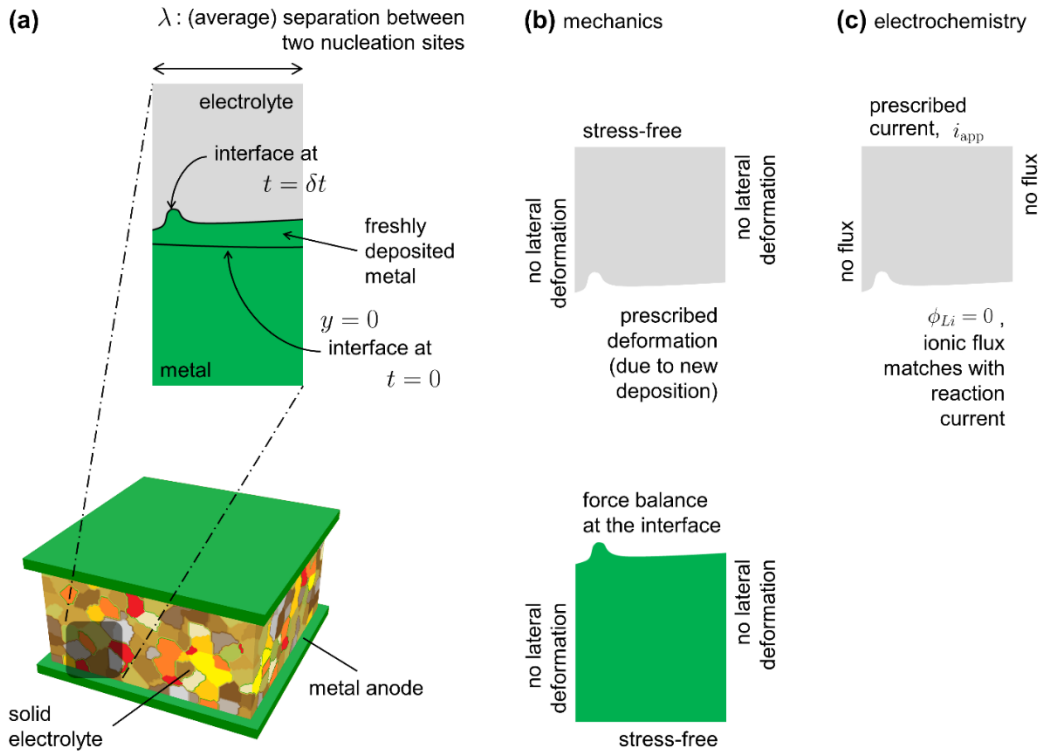

Figure S1. Problem description: Electrodeposition is intrinsically irregular at small lengths comparable to the separation of nucleation sites (a). Such irregular deposition causes perturbation at the metal – electrolyte interface, and the instability of the system reflects in terms of amplifying perturbations. Given the coupling of electrochemical and mechanical interactions, stability analysis involves joint considerations. Appropriate boundary conditions are shown in (b) and (c).

S2. Theoretical Description of Electrodeposition Stability with Solid Electrolytes

The general approach to assessing stability[55-57] introduces a small but finite perturbation to the system and temporally tracks the perturbed profile. The electrodeposition problem differs in two distinct fashions from these well-known instabilities encountered in conventional transport phenomena literature:

- Electrodeposited phase grows, unlike typical instabilities such as Rayleigh-Taylor where there is no mass exchange in-between two adjoining phases. In other words, in traditional settings, interface moves due to advection in fluids or straining in solids, while here interface motion is due to phase growth.
- Given the mesoscopic lengths, local fluctuations are an inherent property of the system and act as a stochastic perturbation field. Hence, instability is not simply an absence of nonuniformity, but rather an arrested growth.

With this background, consider an electrodepositing interface as shown in Figure S1(a). The microscopically discrete nature of the electrodeposition reaction[1] is sketched as a fresh deposition occurring over a small time interval, δt. The associated length-scale, λ, is the representative distance between two adjoining nucleation sites (relates to nucleation site density, $\mathcal{N}_0$). Such an interface evolution occurs due to the phase growth and acts as a prescribed deformation field for the adjacent electrolyte phase. The mechanical contact between the two phases will, in turn, impose a stress field on the new deposits. However, the deformation fields in the adjoining solids do not necessarily match and are an outcome of the force balance at the interface[58]. These mechanical fields, in turn, dictate the evolution of the electrochemical fields and culminate into the reaction, potentials, and ionic flux distributions. Formally, the electrodeposition stability can be expressed as:

> "Given the microscopically discrete nature of the electrodeposition reaction, a stable deposition situation implies that such coarseness does not translate to larger length-scales." (S2)

To better interpret the mechanical state of the interface, visualize two cylindrical specimens of different materials (for example, steel and aluminum; Figure S2(a)) pressed against each other with a pressure, p. Compressive stresses are generated in both the bodies such that every point experiences compressive stress, $\sigma = -p$ (assuming uniform cross-sections). Stresses in the two bodies are balanced at the interface. The difference in elastic properties of the two materials leads to unequal strains and deformations (Figure S2(b)). In other words, for prescribed stress, strains vary with stiffness such that stress components are balanced at the interface. At small length scales, surface energy introduces a jump in normal stresses in response to curvature variations[59] (if surface energy varies along the interface, e.g., due to temperature distribution, tangential stresses at the interface accommodate corresponding gradients).

A growing interface adds further complexity to this as the displacement at the interface is composed of growth and deformation. In general, material motions are matched on either side of the interface and the stresses are balanced (accounting for surface energy effects, if any). For the present situation, the motion of lithium interface is made up of fresh deposition and any deformation due to stresses (Figure S2(e)). On the other hand, the motion of solid electrolyte surface is equal to the motion of the (net) motion of the lithium interface and represents deformation field in the solid electrolyte (bulk motion of solid electrolyte can be neglected at small times). Note that Monroe and Newman's work[5] does not account for

the phase growth in that the interface deformation is identical in both the materials irrespective of their stiffnesses (e.g., Figure S2(d)). This is unphysical since it leads to a considerable force imbalance at the interface. The additional theoretical difference arises from the treatment of stress tensor in reaction kinetics.

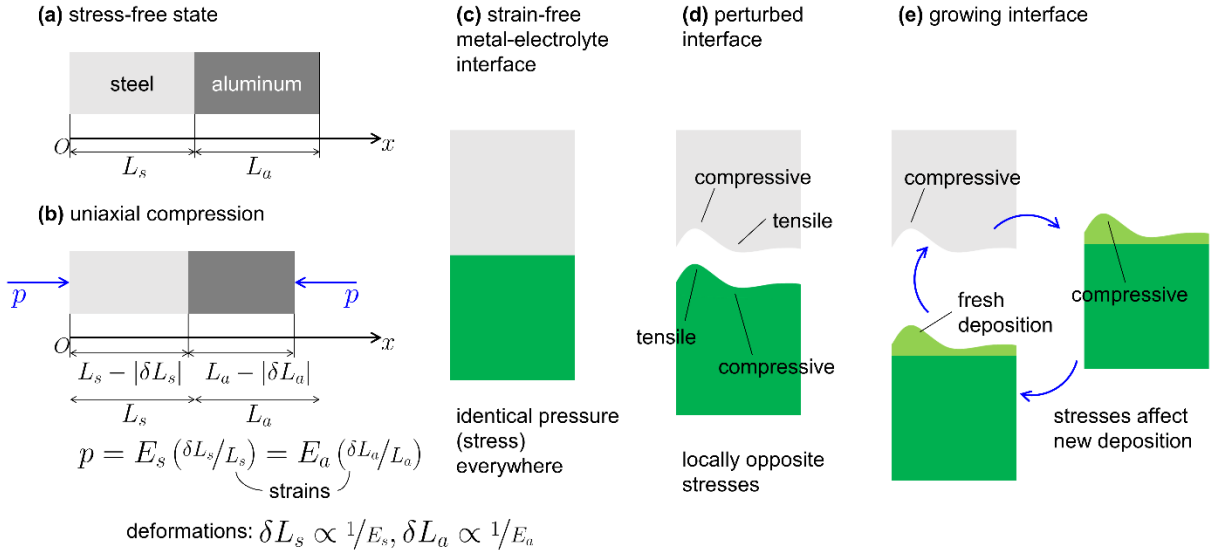

Figure S2. Mechanical state of a solid-solid interface: Schematic illustrations of mechanical state at a solid-solid interface. Geometrical changes at the interface of two solids cylinders as they are compressed (b) from a stress-free state (a). (c) A strain-free metal-electrolyte junction. (d) Perturbed and (e) growing metal-electrolyte interfaces with associated stress fields.

Figure S3(b) and (c) respectively describe the essential boundary and interfacial conditions, while their mathematical forms are prescribed in Table S2. Since the electronic conductivity of the metals is quite higher than the ionic conductivity of the electrolytes, electric potential (i.e., the potential of lithium metal) exhibits negligible variation in the metal as compared to the electrolyte (i.e., potential distribution in the electrolyte phase). In accordance with this, the electrode potential is set to an arbitrarily constant value (zero here), and the electrolyte phase potentials are measured with respect to this reference (as is the conventional interpretation of electrolyte potential[2]). Notice that the ionic flux at the interface needs to be compatible with the reaction current. Relevant governing equations are as follows (in 2D cartesian coordinates):

Mechanical force balance:

$$\frac{\partial \sigma_x}{\partial x} + \frac{\partial \tau_{xy}}{\partial y} = 0 \tag{S3}$$

$$\frac{\partial \sigma_y}{\partial y} + \frac{\partial \tau_{xy}}{\partial x} = 0 \tag{S4}$$

Ionic flux conservation:

$$\frac{\partial i}{\partial x} + \frac{\partial i}{\partial y} = 0 \tag{S5}$$

Stresses are related to displacements via constitutive relations[58]. Here elastic constitutive relations are used. Ionic flux, i (A/m^2) is related to potentials and stresses as discussed subsequently. Hydrostatic stress, σ_{h}, relates to normal stresses, σ, as $\sigma_{\mathrm{h}} = {}^{(\sigma_x+\sigma_y)}/_{2}$. Nomenclature is supplied in Table S3.

Table S2. Physical Constraints: Boundary conditions for stability analysis.

	Boundary Location	Mechanics		Electrochemistry
electrolyte	interface $(y = 0)$	$u = 0$	$v = \frac{\xi}{2}\left(1 + \cos({}^{\pi x}/_{\lambda})\right)$	$i = i_{rxn}$
	lateral faces $(x = 0, \lambda)$	$u = 0$	${}^{\partial v}/_{\partial x} = 0$	${}^{\partial \phi_e}/_{\partial x} = 0$
	far field $(y \gg \lambda)$	${}^{\partial u}/_{\partial y} = 0$	$v = 0$	$i = i_{\mathrm{app}}$
lithium	interface $(y = 0)$	$\sigma_{y,Li} = \sigma_{y,e} - \left(\gamma \frac{\partial^2 v}{\partial x^2}\right)$	$\tau_{Li} = \tau_e$	
	lateral faces $(x = 0, \lambda)$	$u = 0$	${}^{\partial v}/_{\partial x} = 0$	
	far field $(y \ll -\lambda)$	${}^{\partial u}/_{\partial y} = 0$	$v = 0$	

S3. Electrodeposition Kinetics at the Solid – Solid Interface

For any reaction, the observable, i.e., net, behavior results from a competition between reacting tendencies in either direction (Figure S3(a)). The reactivity in each of the directions is characterized by energy barriers, which in turn relate to different energy forms – chemical, electrical, mechanical, etc. A peculiarity of the electrodeposition reactions, e.g., (S6), in contact with a single ion conducting electrolyte is that the ionic concentration is fixed based on the chemical composition of the electrolyte and does not explicitly alter reaction as is common in liquid or polymer electrolytes[1].

$$Li \underset{\text{deposition}}{\overset{\text{dissolution}}{\rightleftharpoons}} Li^{+} + e^{-} \tag{S6}$$

This concentration independence makes instability of the inorganic solid electrolytes, i.e., single-ion conductors, more counterintuitive. The different regimes of irregular electrodeposition in liquid[1, 60-62] and polymer[3, 22, 40] electrolytes fundamentally relate to local ionic depletion. However, in the single-ion conductors, since there is no local ionic depletion, irregular deposition is further confounding.

The statement of thermodynamic equilibrium at the electrochemical interface, i.e., no net current flow, relates to (electro-)chemical potentials[2, 10, 63]. For the electrodeposition reaction (S6):

$$\mu_{Li} = \mu_{Li^+} + \mu_{e^-} \tag{S7}$$

The spontaneity of the reaction relates to reaction free-energy change, $\Delta \mathrm{g}^{rxn}$ as follows (per mole of electron transfer):

$$\Delta \mathrm{g}^{rxn} = \mu_{Li^+} + \mu_{e^-} - \mu_{Li} \tag{S8}$$

The potential landscape for this reaction is schematically shown in Figure S3(b). Even though the reaction spontaneity is related to the net free energy change, $\Delta \mathrm{g}^{rxn}$, reaction rates relate to the activation barriers for respective reaction halves[2, 64]. The three are interdependent as per the identity:

$$\Delta \mathrm{g}^{f} = \Delta \mathrm{g}^{rxn} + \Delta \mathrm{g}^{b} \tag{S9}$$

Here f: forward and b: backward reaction halves. The net reaction rate can be further expressed using the law of mass action for each of the halves (concentration terms are clubbed with the frequency factors given their constant nature in the present context):

$$r = k_f e^{-\Delta \mathrm{g}^{f}/RT} - k_b e^{-\Delta \mathrm{g}^{b}/RT} \tag{S10}$$

Since the free energy terms are expressed on a molar basis, thermal scaling is based on the Universal gas constant, R, rather than the Boltzmann constant, $k_{\mathrm{Boltzmann}}$ (which applies to energy barriers represented per electron). The reaction rate, r, is molar rate per unit electrochemically active surface, i.e., in mol/m^2·s. At equilibrium, the reaction rate becomes zero and provides a relation between the frequency factors. The reaction free energy change, $\Delta \mathrm{g}^{rxn} = 0$ at equilibrium, and in turn (from Eq. (S9)), $\Delta \mathrm{g}^{f,eq} = \Delta \mathrm{g}^{b,eq} = \Delta \mathrm{g}^{eq}$. The activation barriers change for off-equilibrium conditions such that Eq. (S9) is always obeyed. Using this information in (S10), at equilibrium, $k_f e^{-\Delta \mathrm{g}^{eq}/RT} = k_b e^{-\Delta \mathrm{g}^{eq}/RT} = k$. Substituting for these in the rate expression (S10):

$$r = k\left\{e^{-\left(\Delta \mathrm{g}^{f} - \Delta \mathrm{g}^{eq}\right)/RT} - e^{-\left(\Delta \mathrm{g}^{b} - \Delta \mathrm{g}^{eq}\right)/RT}\right\} \tag{S11}$$

Here $\Delta \mathrm{g}^{eq}$ is the activation barrier at equilibrium, while $\left(\Delta \mathrm{g}^{f} - \Delta \mathrm{g}^{eq}\right)$ and $\left(\Delta \mathrm{g}^{b} - \Delta \mathrm{g}^{eq}\right)$ are partitions of reaction spontaneity, $\Delta \mathrm{g}^{rxn}$, that contribute to each of the halves.

The (electro)chemical potential of the interacting entities are mathematically expressed as:

$$\mu_{Li} = \mu_{Li}^{\circ} - \Omega_{Li}\sigma_{\mathrm{h},Li} \tag{S12}$$

$$\mu_{Li^+} = \mu_{Li^+}^{\circ} + F\phi_e - \Omega_{Li^+}\sigma_{\mathrm{h},e} \tag{S13}$$

$$\mu_{e^-} = \mu_{e^-}^{\circ} - F\phi_s \tag{S14}$$

where the reference values refer to standard temperature and pressure as well as absorb the concentration dependence since it is constant for a single ion conducting electrolyte. Only extra hydrostatic stresses affect chemical potential[65]. Here in compressive stresses are treated negative, while tensile stresses are treated positive. Substituting (S12) through (S14) in reaction free energy expression (S8):

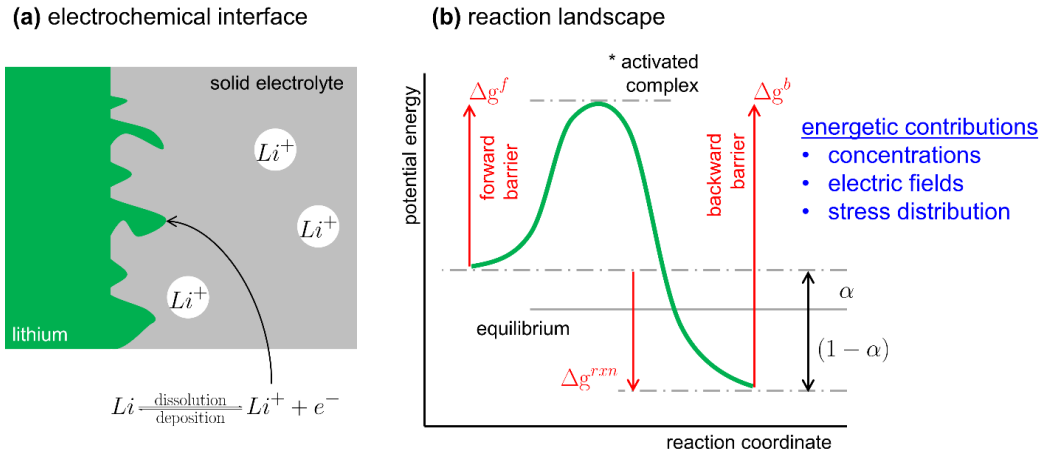

Figure S3. Energic picture of reaction kinetics: (a) Microscopic view of the electrochemical interface. (b) Energy landscape for the electrodeposition reaction. Different physicochemical factors contributing to reaction kinetics are also mentioned.

$$\Delta \mathrm{g}^{rxn} = \{\mu^\circ_{Li^+} + F\phi_e - \Omega_{Li^+}\sigma_{\mathrm{h},e}\} + \{\mu^\circ_{e^-} - F\phi_s\} - \{\mu^\circ_{Li} - \Omega_{Li}\sigma_{\mathrm{h},Li}\}$$

$$\therefore \Delta \mathrm{g}^{rxn} = \{\mu^\circ_{Li^+} + \mu^\circ_{e^-} - \mu^\circ_{Li^+}\} + F(\phi_e - \phi_s) - \{\Omega_{Li^+}\sigma_{\mathrm{h},e} - \Omega_{Li}\sigma_{\mathrm{h},Li}\}$$

or,

$$\Delta \mathrm{g}^{rxn} = -F\eta_\phi - F\eta_\sigma \tag{S15}$$

$$\eta_\phi = \phi_s - \phi_e - U \tag{S16}$$

$$\eta_\sigma = \frac{1}{F}\{\Omega_{Li^+}\sigma_{\mathrm{h},e} - \Omega_{Li}\sigma_{\mathrm{h},Li}\} \tag{S17}$$

$$U = \mu^\circ_{Li^+} + \mu^\circ_{e^-} - \mu^\circ_{Li} \tag{S18}$$

where the reaction spontaneity has contributions from electric (η_ϕ) and mechanical (η_σ) fields. The partition of both these effects need not be identical. It has been usually observed that the electric field spontaneity equally applies to the anodic and cathodic halves, while the mechanical fields contribute primarily to the anodic reaction[14]. The reaction rate expression accordingly simplifies to:

$$r = k\left\{e^{F\eta_\sigma/RT}e^{F\eta_\phi/2RT} - e^{-F\eta_\phi/2RT}\right\} \tag{S19}$$

In terms of reaction current,

$$i_{rxn} = Fr = i_0 \left\{ e^{F\eta_\sigma/RT} e^{F\eta_\phi/2RT} - e^{-F\eta_\phi/2RT} \right\} \quad \text{(S20)}$$

Note that the stress overpotential, η_σ, involves the partial molar volume of cation, Ω_{Li^+}, molar volume of lithium, Ω_{Li}, the hydrostatic stress in the electrolyte, $\sigma_{\mathrm{h},e}$, and the hydrostatic stress in lithium, $\sigma_{\mathrm{h},Li}$. In the limit of vanishing stress field, $\eta_\sigma \to 0$, and in turn, the kinetic expression reduces to the conventional Butler-Volmer[2]. The cationic partial molar volume, Ω_{Li^+}, refers to the increase in cationic free energy when unit isotropic compressive stress is applied as compared to the stress-free state of the electrolyte. This approach to deriving a consistent kinetic expression is philosophically identical to that employed literature for different electrochemical reactions[2, 66].

S4. Physical Interpretation of (Partial) Molar Volume

Partial molar volumes are difficult to measure[14]. To make matters worse, three different interpretation (definitions) are available[67] with little or no discussion on their equivalence.

- Ionic volume: relates to the radius of the ion of interest in the solution environment, e.g.,[44-45]
- Geometrical volume change: defined as the difference in volume with changes in species concentration; often used in chemo-mechanical effects for active particles in electrodes, e.g.,[68-73]
- Stress energy volume: defined as a change in (electro-)chemical potential for a unit change in stress[65, 67]

Ionic radius is defined as the distance between the nucleus and the outer most shell of electrons[64] for a given ion. Microscopically every material is made up of voids and ionic and/or atomic arrangements. Hence, the ionic volume does not correlate to macroscopic volume.

Geometrical volume is the most common interpretation and in principle easy to measure. It relates to mechanical strains in active particles like graphite and silicon and porosity variations in precipitation-dissolution electrodes such as Li-sulfur[73] and Li-air[74]. It is usually argued that the volume change of inorganic solid electrolytes is negligible upon addition of lithium, and in turn partial molar volume of lithium cations is almost zero[75]. However, both lithium-free and lithiated states, e.g., $La_3Zr_2O_{12}$ and $Li_7La_3Zr_2O_{12}$, are charge-neutral, and the volume change does not relate to the volume of Li^+. Secondly, such a straightforward interpretation assumes that ideal solutions are formed where volumes of individual species are additive. Ideal solution assumption is often not valid except in very dilute conditions.

The stress energy volume is difficult to measure because (electro-)chemical potentials cannot be measured directly (appropriate stress state can be achieved easily). The stress energy volume is the relevant descriptor for present discussion as the mechanical asymmetry in reaction kinetics (Eq. (S20)) is defined based on changes in (electro-)chemical

potential induced by mechanical stresses. Liquids cannot sustain shear and as a result, partial molar volume is a scalar, $\Omega = {}^{\partial\mu}/_{\partial p}|_{T,c}$, where pressure, p, defines the stressed state. On the other hand, solids can sustain shear and in general, partial molar volume is a second-order tensor, $\Omega_{i,j} = -{}^{\partial\mu}/_{\partial\sigma_{i,j}}|_{T,c}$, where each entry $\Omega_{i,j}$ refers to the corresponding stress component, $\sigma_{i,j}$. For isotropic solutes, shear stresses do not contribute to (electro-)chemical potentials and the partial molar volume reduces to a scalar value related to the hydrostatic stress, i.e., $\Omega = -{}^{\partial\mu}/_{\partial\sigma_h}|_{T,c}$. Lithium ions, given the spherical symmetry, can be assumed as isotropic solutes.

For ideal gases, the geometrical and stress energy descriptions refer to the same quantity[76] (volume of one mole of gases; note that atomic volume in an ideal gas is zero). Given the analytically equivalent forms of (partial) molar volume expressions for gaseous, liquid and solid states, it is usually assumed that the two are identical. Such an equivalence is justified for pure phases, i.e., for molar volumes[10, 63, 77]. However, for non-ideal mixtures (e.g., water-ethanol[78]), concentrated and/or ionic solutes, it cannot be justified, and the two values can differ.

Such differences do not necessarily imply any inconsistency. It is possible that for a given amount of solute (here ions), change in geometrical dimension and energy are not correlated. Strictly speaking, any interactions derived based on non-equilibrium thermodynamics employs (electro-)chemical potential and in turn stress energy-based partial molar volumes should be used. Reaction kinetics and species transport are representative non-equilibrium interactions.

S5. Charge Transfer Resistance of a Stressed Electrochemical Interface

Often experimental probing of solid electrolytes[20-21, 30-31, 34, 53] characterizes the reacting interface using impedance spectroscopy which provides a value for the charge transfer resistance, R_{ct}. The interpretation of R_{ct} is related to the analytical form of the reaction kinetics[79]. Consider a prestressed interface as shown in Figure S4. It represents a situation of uniform hydrostatic stress resulting from the external pressure, p, i.e., $\sigma_e = \sigma_s = -p$. Accordingly, the stress overpotential simplifies to:

$$\eta_\sigma = \frac{p\Omega_{Li}}{F}\left(1 - {}^{\Omega_{Li^+}}/_{\Omega_{Li}}\right) \tag{S21}$$

Using the kinetic expression (S20), the open circuit condition (no current flow) relates the two overpotentials as $\eta_\phi + \eta_\sigma = 0$. The charge transfer resistance refers to a small electrical perturbation about this equilibrium state:

$$R_{\text{ct}} = \frac{\partial\eta_\phi}{\partial i_{rxn}} = \frac{2RT}{Fi_0\left\{e^{F\eta_\sigma/RT}e^{F\eta_\phi/2RT} + e^{-F\eta_\phi/2RT}\right\}} = \frac{RT}{Fi_0}e^{-F\eta_\sigma/2RT}$$

$$\therefore R_{\mathrm{ct}} = \frac{RT}{Fi_0} \exp\left(\frac{p\Omega_{Li}}{2RT}\left(\Omega_{Li^+}/\Omega_{Li} - 1\right)\right) \tag{S22}$$

And the relationship between the potential jump across the interface relates to pressure as:

$$\phi_s - \phi_e - U = \frac{p\Omega_{Li}}{F}\left(\Omega_{Li^+}/\Omega_{Li} - 1\right) \tag{S23}$$

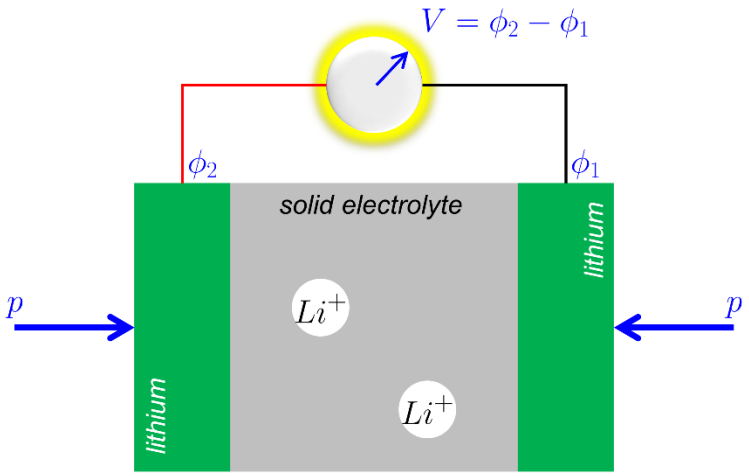

Figure S4. Physical state during Impedance probing: Impedance measurements are carried out in an equilibrium condition (i.e., open circuit). It represents a state of no current flow as well as no displacement due to acting compressive stresses (i.e., pressure).

Under the same applied pressure, when the contact resistance decreases, it indicates a reduction in cationic partial molar volume as per the expression (S22). However, the open circuit voltage measurement does not detect such an interfacial signature:

$$V = \phi_2 - \phi_1 = \left\{\phi_e + U + \frac{p\Omega_{Li}}{F}\left(\frac{\Omega_{Li^+}}{\Omega_{Li}} - 1\right)\right\}_2 - \left\{\phi_e + U + \frac{p\Omega_{Li}}{F}\left(\frac{\Omega_{Li^+}}{\Omega_{Li}} - 1\right)\right\}_1 \tag{S24}$$

Reduction in charge transfer resistance is usually termed as improved interfacial wetting. Expression (S22) reveals that interfacial wetting fundamentally relates to the cationic partial molar volume at the interface, which in turn is strongly dependent on the structural – crystallographic arrangement.

S6. Non-equilibrium Charge Transport in a Solid Electrolyte

As mentioned earlier, the transport in (inorganic) solid electrolytes differs from the liquid or polymer electrolytes where all the ionic charge is motile. The inorganic solid electrolytes, on the other hand, have a negatively charged matrix which hosts the mobile cations. The overall

electrolyte is always charge neutral. Microscopically, the cations (here Li^+) move via hopping. Necessary energy for such microscopic jumps is either facilitated by thermal energy and interspecies forces[80-82] (van der Waals, coulombic, etc.). When such molecular description (e.g., MD calculations) is scaled up to larger lengths, a continuum picture emerges where the non-equilibrium interactions are described by Onsager Stefan Maxwell (OSM) relation:

$$-\frac{c_{Li^+}c_\Sigma}{RT}\nabla\mu_{Li^+} = \frac{c_m N_{Li^+} - c_{Li^+}N_m}{D_{+m}} \tag{S25}$$

where N's are molar species fluxes and 'm' is the background matrix phase. D_{+m} is the binary diffusivity of the cation in the background matrix (microscopically resulting from the hopping mechanism). Given that the matrix phase is stagnant, $N_m = 0$. Rearranging (S25) accordingly,

$$N_{Li^+} = -\frac{D_{+m}}{RT}\cdot\frac{c_{Li^+}c_\Sigma}{c_m}\nabla\mu_{Li^+} \tag{S26}$$

Substituting for the electrochemical potential of the cation from Eq. (S13),

$$N_{Li^+} = -\frac{D_{+m}}{RT}\cdot\frac{c_{Li^+}c_\Sigma}{c_m}\nabla\left(\mu^\circ_{Li^+} + F\phi_e - \Omega_{Li^+}\sigma_{\mathrm{h},Li^+}\right)$$

or,

$$i = FN_{Li^+} = -\kappa\nabla\phi_e - \kappa_\sigma\nabla\sigma_{\mathrm{h},e} \tag{S27}$$

$$\kappa = F^2\frac{D_{+m}}{RT}\cdot\frac{c_{Li^+}c_\Sigma}{c_m} \tag{S28}$$

$$\frac{\kappa_\sigma}{\kappa} = {}^{-\Omega_{Li^+}}/_{F} \tag{S29}$$

where the stress conductivity κ_σ represents alteration to the ionic flux in response to the local hydrostatic stress field. The ionic conductivity is routinely inferred from the impedance spectra. As discussed in Figure S4, under an open circuit condition, the hydrostatic stress field is uniform, and in turn, the stress-dependent ionic current is not captured in conventional experimental settings. However, during irregular electrodeposition, the uneven stress field is generated and the stress-driven-conduction takes place.

Notice that the ionic motion is diffusive[37, 83] in nature (probably through some form of hopping mechanism) but does not lead to concentration gradients, given the charge neutrality and stoichiometry of the structural arrangement.

S7. Unusual Lithium Growth in Polymer Electrolyte

Polymer electrolytes are much softer than lithium and consequently, the theoretical analysis usually predicts unstable electrodeposition growth[5, 42, 44]. However, such a claim of

mechanically-induced instability is difficult to prove experimentally, in part due to the existence of mass-transport instability in such electrolytes[6, 22, 40]. Mass transport instability becomes less dominant for thinner electrolytes and currents smaller than limiting current[1], and one should be able to distinguish the mechanical interplay.

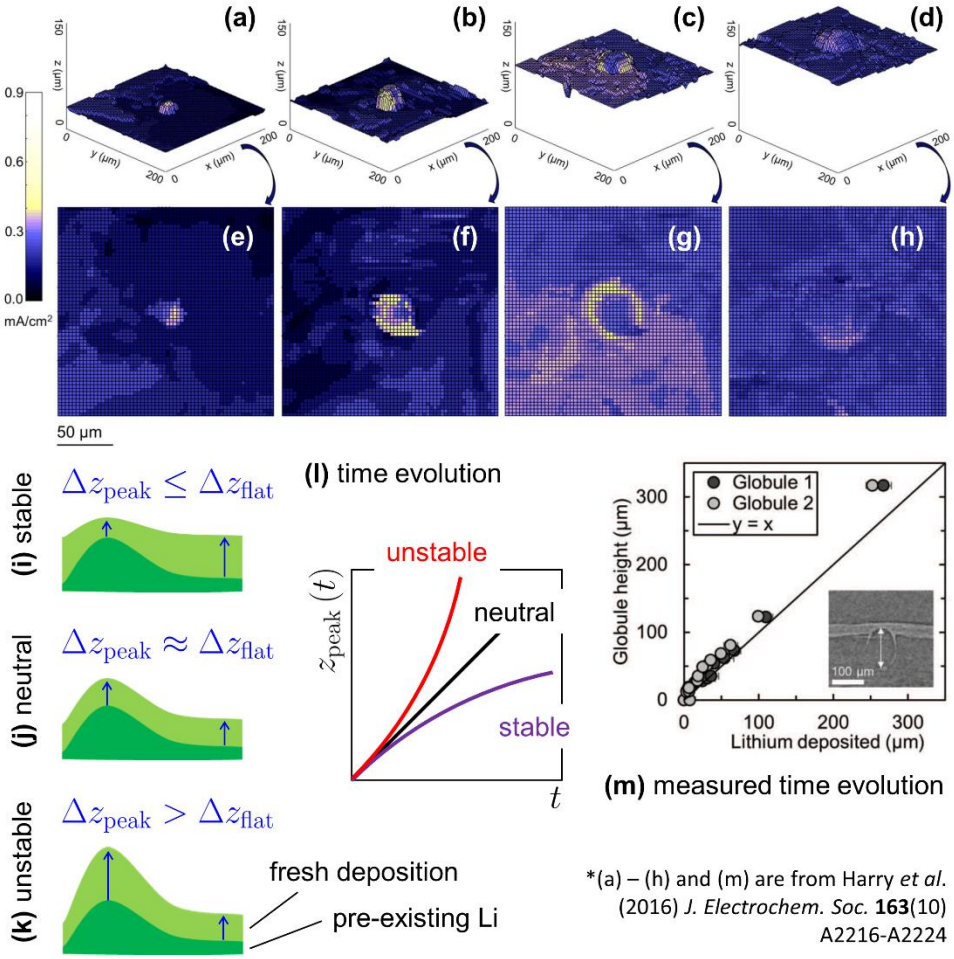

Figure S5. Electrodeposition with Polymer Electrolyte: Tomographic measurements[23] of growing lithium protrusion in polystyrene-*b*-poly(ethylene oxide). (a) through (d) show reconstructed lithium – electrolyte interface after depositing (a) 0 (b) 8.27 (c) 16.53 and (d) 35.82 C/cm^2. (e) through (h) retrieve local current density using two consecutive time snaps and Faraday's law; (e) 0 – 8.27 C/cm^2, (f) 8.27 – 16.53 C/cm^2, (g) 16.53 – 35.82 C/cm^2 and (h) 35.82 – 54.72 C/cm^2 intervals. Schematic illustration of (i) stable (j) neutral and (k) unstable growth, and equivalent (l) time evolution of the protrusion height. (m) Protrusion height measured from tomographic measurements[23]. (a) – (h) and (m) are reproduced from Harry *et al.* (2016) *J. Electrochem. Soc.* **163**(10) A2216-A2224 with permission from authors under the Creative Commons license.

Figure S5 reports a recent experimental study[23] of galvanostatic (constant current) electrodeposition with thin polymer electrolyte (~30 μm). The current is smaller than the (theoretical) limiting current that could trigger irregular growth due to mass-transport instability. Figure S5(a)-(d) reproduces tomographic reconstruction of the depositing

lithium – electrolyte interface. Uneven growth originates from an impurity particle present at the surface of lithium metal film. As per the conventional interpretation[5, 42, 44], polymer electrolyte is quite soft to arrest irregular growth. Reaction current should stay focused at the tip of the protrusion (mass-transport limitations, if present, would further support this tendency). However, analysis of consecutive tomograms[23] reveals that the initial focusing of the reaction current gradually subsides and at late times reaction distribution becomes uniform (Figure S5(e)-(h)). In other words, the growth rate of protrusion gradually decreases (i.e., arrested). If the electrodeposition were unstable, growth would rather accelerate. Figure S5(i)-(k) sketches successive interface locations for (i) stable (j) neutral and (k) unstable growth. A neutral growth (Figure S5(j)) refers to spatially uniform deposition. The interface motions for these three scenarios are collectively shown in Figure S5(l) to provide a comparison against the measured signature (Figure S5(m)). Figure S5(m) suggests that the protrusion growth is not unstable.

This study provides a peculiar set of observations where irregular growth is arrested even with a soft electrolyte.

Table S3. Nomenclature: The list of symbols used in the discussion.

Symbol	Description	Value (Units)
D_{+m}	cation diffusivity in the solid electrolyte	(m^2/s)
e^-	electron	
F	Faraday's constant	96487 (C/mol)
G	shear modulus	(GPa)
g	Gibb's free energy	(J/mol)
i	current density	(A/m^2)
i_0	exchange current density	50 (A/m^2)
j_b	flux bending	(kJ/mol·m)
k	reaction rate	($mol/m^2{\cdot}s$)
N	molar flux	($mol/m^2{\cdot}s$)
$\mathcal{N}_0$	nucleation site density	10^{12} ($\#/m^2$)
$\mathcal{O}$	of the order of; represents scales of quantities	
p	pressure	(Pa)
R	Universal gas constant	8.314 (J/mol·K)
R_ct	charge transfer resistance	(Ωm^2)
T	temperature	298.15 (K)
t	time	(s)
U	open circuit potential	(V)
u	longitudinal deformation	(m)

v	transverse deformation	(m)
x	longitudinal coordinate	(m)
y	transverse coordinate	(m)
Greek Symbols:		
α	fractional contribution to the forward reaction barrier	-
γ	interfacial (surface) energy	10^{-3} to 1 (N/m)
Δ	difference, e.g., maximum and minimum values *or* departure from a reference state	
δ	small (infinitesimal) change	
η	overpotential	(V)
Θ	stability quotient	-
κ	ionic conductivity	(S/m)
κ_σ	stress conductivity	(A/Pa·m)
$\varkappa$	curvature	(1/m)
λ	average separation between nucleation sites; relates to nucleation site density as $\lambda \sim {}^{1}/_{\mathcal{N}_0}$	10^{-6} (m)
μ	(electro-) chemical potential	(J/mol)
ν	Poisson's ratio	-
ξ	perturbation amplitude at the interface	25 (nm)
σ	normal stress	(Pa)
σ_{h}	hydrostatic stress	(Pa)
τ	shear stress	(Pa)
ϕ	potential	(V)
ψ^*	critical distortion	(-)
ψ	distortion	-
Ω	(partial) molar volume	m^3/mol
Superscripts/ Subscripts:		
b	backward reaction half	
e	solid electrolyte	
f	forward reaction half	
Li	lithium metal	
Li^+	lithium ion (cation)	
m	electrolyte matrix: solid electrolyte consists of cations in the background ceramic matrix	
rxn	reaction, i.e., electrodeposition at the interface	
t	ionic transport in the solid electrolyte	
x	longitudinal direction	

y	transverse direction	
$+$	cation	
$\circ$	reference property	
σ	stress effect	
ϕ	potential effect	
Abbreviations:		
LAGP	Aluminum – Germanium Phosphate, e.g., $Li_{1.4}Al_{0.4}Ge_{1.6}(PO_4)_3$	
LGPS	Germanium – Phosphorus Sulfide, e.g., $Li_{10}GeP_2S_{12}$	
LLZO	Lanthanum – Zirconium Oxide, e.g., $Li_7La_3Zr_2O_{12}$	
LPS	Phosphate based solid electrolyte, e.g., γ-Li_3PS_4	
MD	Molecular Dynamics	
OCP	Open Circuit Potential	
OSM	Onsager – Stefan – Maxwell description for nonequilibrium transport	

References

(1) Mistry, A.; Fear, C.; Carter, R.; Love, C. T.;Mukherjee, P. P. Electrolyte Confinement Alters Lithium Electrodeposition. *ACS Energy Lett.* **2019**, *4*, 156-162.

(2) Newman, J.;Thomas-Alyea, K. E. *Electrochemical Systems*; John Wiley & Sons: New Jersey, 2012.

(3) Monroe, C.;Newman, J. Dendrite Growth in Lithium/Polymer Systems a Propagation Model for Liquid Electrolytes under Galvanostatic Conditions. *J. Electrochem. Soc.* **2003**, *150*, A1377-A1384.

(4) Qian, J.; Henderson, W. A.; Xu, W.; Bhattacharya, P.; Engelhard, M.; Borodin, O.;Zhang, J.-G. High Rate and Stable Cycling of Lithium Metal Anode. *Nature communications* **2015**, *6*, 6362.

(5) Monroe, C.;Newman, J. The Impact of Elastic Deformation on Deposition Kinetics at Lithium/Polymer Interfaces. *J. Electrochem. Soc.* **2005**, *152*, A396-A404.

(6) Pesko, D. M.; Feng, Z.; Sawhney, S.; Newman, J.; Srinivasan, V.;Balsara, N. P. Comparing Cycling Characteristics of Symmetric Lithium-Polymer-Lithium Cells with Theoretical Predictions. *J. Electrochem. Soc.* **2018**, *165*, A3186-A3194.

(7) Harry, K. J.; Hallinan, D. T.; Parkinson, D. Y.; MacDowell, A. A.;Balsara, N. P. Detection of Subsurface Structures Underneath Dendrites Formed on Cycled Lithium Metal Electrodes. *Nat. Mater.* **2014**, *13*, 69.

(8) Rosso, M.; Gobron, T.; Brissot, C.; Chazalviel, J.-N.;Lascaud, S. Onset of Dendritic Growth in Lithium/Polymer Cells. *J. Power Sources* **2001**, *97*, 804-806.

(9) Rosso, M.; Brissot, C.; Teyssot, A.; Dollé, M.; Sannier, L.; Tarascon, J.-M.; Bouchet, R.;Lascaud, S. Dendrite Short-Circuit and Fuse Effect on Li/Polymer/Li Cells. *Electrochim. Acta* **2006**, *51*, 5334-5340.

(10) De Groot, S. R.;Mazur, P. *Non-Equilibrium Thermodynamics*; Courier Corporation, 2013.

(11) Guo, L.; Oskam, G.; Radisic, A.; Hoffmann, P. M.;Searson, P. C. Island Growth in Electrodeposition. *J. Phys. D: Appl. Phys.* **2011**, *44*, 443001.

(12) Sun, F.; Osenberg, M.; Dong, K.; Zhou, D.; Hilger, A.; Jafta, C. J.; Risse, S.; Lu, Y.; Markötter, H.;Manke, I. Correlating Morphological Evolution of Li Electrodes with Degrading Electrochemical Performance of Li/Licoo2 and Li/S Battery Systems: Investigated by Synchrotron X-Ray Phase Contrast Tomography. *ACS Energy Lett.* **2018**, *3*, 356-365.

(13) Paunovic, M.;Schlesinger, M. *Fundamentals of Electrochemical Deposition*; john wiley & sons, 2006; Vol. 45.

(14) Monroe, C.;Newman, J. The Effect of Interfacial Deformation on Electrodeposition Kinetics. *J. Electrochem. Soc.* **2004**, *151*, A880-A886.

(15) Cheng, E. J.; Sharafi, A.;Sakamoto, J. Intergranular Li Metal Propagation through Polycrystalline Li6. 25al0. 25la3zr2o12 Ceramic Electrolyte. *Electrochim. Acta* **2017**, *223*, 85-91.

(16) Porz, L.; Swamy, T.; Sheldon, B. W.; Rettenwander, D.; Frömling, T.; Thaman, H. L.; Berendts, S.; Uecker, R.; Carter, W. C.;Chiang, Y. M. Mechanism of Lithium Metal Penetration through Inorganic Solid Electrolytes. *Adv. Energy Mater.* **2017**, *7*, 1701003.

(17) Lewis, J. A.; Cortes, F. J. Q.; Boebinger, M. G.; Tippens, J.; Marchese, T. S.; Kondekar, N. P.; Liu, X.; Chi, M.;McDowell, M. T. Interphase Morphology between a Solid-State Electrolyte and Lithium Controls Cell Failure. *ACS Energy Lett.* **2019**.

(18) Li, Y.; Zhou, W.; Chen, X.; Lü, X.; Cui, Z.; Xin, S.; Xue, L.; Jia, Q.;Goodenough, J. B. Mastering the Interface for Advanced All-Solid-State Lithium Rechargeable Batteries. *Proceedings of the National Academy of Sciences* **2016**, *113*, 13313-13317.

(19) Wu, B.; Wang, S.; Lochala, J.; Desrochers, D.; Liu, B.; Zhang, W.; Yang, J.;Xiao, J. The Role of the Solid Electrolyte Interphase Layer in Preventing Li Dendrite Growth in Solid-State Batteries. *Energy Environ. Sci.* **2018**, *11*, 1803-1810.

(20) Luo, W.; Gong, Y.; Zhu, Y.; Fu, K. K.; Dai, J.; Lacey, S. D.; Wang, C.; Liu, B.; Han, X.;Mo, Y. Transition from Superlithiophobicity to Superlithiophilicity of Garnet Solid-State Electrolyte. *J. Am. Chem. Soc.* **2016**, *138*, 12258-12262.

(21) Han, X.; Gong, Y.; Fu, K. K.; He, X.; Hitz, G. T.; Dai, J.; Pearse, A.; Liu, B.; Wang, H.;Rubloff, G. Negating Interfacial Impedance in Garnet-Based Solid-State Li Metal Batteries. *Nat. Mater.* **2017**, *16*, 572.

(22) Maslyn, J. A.; Loo, W. S.; McEntush, K. D.; Oh, H. J.; Harry, K. J.; Parkinson, D. Y.;Balsara, N. P. Growth of Lithium Dendrites and Globules through a Solid Block Copolymer Electrolyte as a Function of Current Density. *J. Phys. Chem. C* **2018**, *122*, 26797-26804.

(23) Harry, K. J.; Higa, K.; Srinivasan, V.;Balsara, N. P. Influence of Electrolyte Modulus on the Local Current Density at a Dendrite Tip on a Lithium Metal Electrode. *J. Electrochem. Soc.* **2016**, *163*, A2216-A2224.

(24) Swamy, T.; Park, R.; Sheldon, B. W.; Rettenwander, D.; Porz, L.; Berendts, S.; Uecker, R.; Carter, W. C.;Chiang, Y.-M. Lithium Metal Penetration Induced by Electrodeposition through Solid Electrolytes: Example in Single-Crystal Li6la3zrtao12 Garnet. *J. Electrochem. Soc.* **2018**, *165*, A3648-A3655.

(25) Bucci, G.; Talamini, B.; Balakrishna, A. R.; Chiang, Y.-M.;Carter, W. C. Mechanical Instability of Electrode-Electrolyte Interfaces in Solid-State Batteries. *Physical Review Materials* **2018**, *2*, 105407.

(26) Swamy, T.; Chen, X.;Chiang, Y.-M. Electrochemical Redox Behavior of Li-Ion Conducting Sulfide Solid Electrolytes. *Chem. Mater.* **2019**.

(27) Ganser, M.; Hildebrand, F. E.; Klinsmann, M.; Hanauer, M.; Kamlah, M.;McMeeking, R. M. An Extended Formulation of Butler-Volmer Electrochemical Reaction Kinetics Including the Influence of Mechanics. *J. Electrochem. Soc.* **2019**, *166*, H167-H176.

(28) McMeeking, R. M.; Ganser, M.; Klinsmann, M.;Hildebrand, F. E. Metal Electrode Surfaces Can Roughen Despite the Constraint of a Stiff Electrolyte. *J. Electrochem. Soc.* **2019**, *166*, A984-A995.

(29) Li, G.;Monroe, C. W. Dendrite Nucleation in Lithium-Conductive Ceramics. *Phys. Chem. Chem. Phys.* **2019**, *21*, 20354-20359.

(30) Taylor, N. J.; Stangeland-Molo, S.; Haslam, C. G.; Sharafi, A.; Thompson, T.; Wang, M.; Garcia-Mendez, R.;Sakamoto, J. Demonstration of High Current Densities and Extended Cycling in the Garnet Li 7 La 3 Zr 2 O 12 Solid Electrolyte. *J. Power Sources* **2018**, *396*, 314-318.

(31) Smith, S.; Thompson, T.; Sakamoto, J.; Allen, J. L.; Baker, D. R.;Wolfenstine, J. Electrical, Mechanical and Chemical Behavior of Li1. 2zr1. 9sr0. 1 (Po4) 3. *Solid State Ionics* **2017**, *300*, 38-45.

(32) Garcia-Mendez, R.; Mizuno, F.; Zhang, R.; Arthur, T. S.;Sakamoto, J. Effect of Processing Conditions of 75li2s-25p2s5 Solid Electrolyte on Its Dc Electrochemical Behavior. *Electrochim. Acta* **2017**, *237*, 144-151.

(33) Ma, C.; Cheng, Y.; Yin, K.; Luo, J.; Sharafi, A.; Sakamoto, J.; Li, J.; More, K. L.; Dudney, N. J.;Chi, M. Interfacial Stability of Li Metal–Solid Electrolyte Elucidated Via in Situ Electron Microscopy. *Nano Lett.* **2016**, *16*, 7030-7036.

(34) Kim, Y.; Yoo, A.; Schmidt, R.; Sharafi, A.; Lee, H.; Wolfenstine, J.;Sakamoto, J. Electrochemical Stability of Li6.5la3zr1.5m0.5o12 (M = Nb or Ta) against Metallic Lithium. *Frontiers in Energy Research* **2016**, *4*.

(35) Yu, S.;Siegel, D. J. Grain Boundary Softening: A Potential Mechanism for Lithium Metal Penetration through Stiff Solid Electrolytes. *ACS Appl. Mater. Interfaces* **2018**, *10*, 38151-38158.

(36) Sharafi, A.; Kazyak, E.; Davis, A. L.; Yu, S.; Thompson, T.; Siegel, D. J.; Dasgupta, N. P.;Sakamoto, J. Surface Chemistry Mechanism of Ultra-Low Interfacial Resistance in the Solid-State Electrolyte Li7la3zr2o12. *Chem. Mater.* **2017**, *29*, 7961-7968.

(37) Yu, S.;Siegel, D. J. Grain Boundary Contributions to Li-Ion Transport in the Solid Electrolyte Li7la3zr2o12 (Llzo). *Chem. Mater.* **2017**, *29*, 9639-9647.

(38) Thompson, T.; Yu, S.; Williams, L.; Schmidt, R. D.; Garcia-Mendez, R.; Wolfenstine, J.; Allen, J. L.; Kioupakis, E.; Siegel, D. J.;Sakamoto, J. Electrochemical Window of the Li-Ion Solid Electrolyte Li7la3zr2o12. *ACS Energy Lett.* **2017**, *2*, 462-468.

(39) Yu, S.; Schmidt, R. D.; Garcia-Mendez, R.; Herbert, E.; Dudney, N. J.; Wolfenstine, J. B.; Sakamoto, J.;Siegel, D. J. Elastic Properties of the Solid Electrolyte Li7la3zr2o12 (Llzo). *Chem. Mater.* **2015**, *28*, 197-206.

(40) Barai, P.; Higa, K.;Srinivasan, V. Impact of External Pressure and Electrolyte Transport Properties on Lithium Dendrite Growth. *J. Electrochem. Soc.* **2018**, *165*, A2654-A2666.

(41) Srinivasan, V.; Higa, K.; Barai, P.;Xie, Y. Computational Modeling of Morphology Evolution in Metal-Based Battery Electrodes. *Handbook of Materials Modeling: Methods: Theory and Modeling* **2018**, 1-27.

(42) Barai, P.; Higa, K.;Srinivasan, V. Lithium Dendrite Growth Mechanisms in Polymer Electrolytes and Prevention Strategies. *Phys. Chem. Chem. Phys.* **2017**, *19*, 20493-20505.

(43) Barai, P.; Higa, K.;Srinivasan, V. Effect of Initial State of Lithium on the Propensity for Dendrite Formation: A Theoretical Study. *J. Electrochem. Soc.* **2017**, *164*, A180-A189.

(44) Ahmad, Z.;Viswanathan, V. Stability of Electrodeposition at Solid-Solid Interfaces and Implications for Metal Anodes. *Phys. Rev. Lett.* **2017**, *119*, 056003.

(45) Ahmad, Z.;Viswanathan, V. Role of Anisotropy in Determining Stability of Electrodeposition at Solid-Solid Interfaces. *Physical Review Materials* **2017**, *1*, 055403.

(46) Ahmad, Z.; Xie, T.; Maheshwari, C.; Grossman, J. C.;Viswanathan, V. Machine Learning Enabled Computational Screening of Inorganic Solid Electrolytes for Suppression of Dendrite Formation in Lithium Metal Anodes. *ACS Cent. Sci.* **2018**, *4*, 996-1006.

(47) Yang, C.; Zhang, L.; Liu, B.; Xu, S.; Hamann, T.; McOwen, D.; Dai, J.; Luo, W.; Gong, Y.;Wachsman, E. D. Continuous Plating/Stripping Behavior of Solid-State Lithium Metal Anode in a 3d Ion-Conductive Framework. *Proceedings of the National Academy of Sciences* **2018**, *115*, 3770-3775.

(48) Wang, C.; Xie, H.; Zhang, L.; Gong, Y.; Pastel, G.; Dai, J.; Liu, B.; Wachsman, E. D.;Hu, L. Universal Soldering of Lithium and Sodium Alloys on Various Substrates for Batteries. *Adv. Energy Mater.* **2018**, *8*, 1701963.

(49) Fu, K.; Gong, Y.; Fu, Z.; Xie, H.; Yao, Y.; Liu, B.; Carter, M.; Wachsman, E.;Hu, L. Transient Behavior of the Metal Interface in Lithium Metal–Garnet Batteries. *Angew. Chem. Int. Ed.* **2017**, *56*, 14942-14947.

(50) Fu, K. K.; Gong, Y.; Liu, B.; Zhu, Y.; Xu, S.; Yao, Y.; Luo, W.; Wang, C.; Lacey, S. D.;Dai, J. Toward Garnet Electrolyte–Based Li Metal Batteries: An Ultrathin, Highly Effective, Artificial Solid-State Electrolyte/Metallic Li Interface. *Sci. Adv.* **2017**, *3*, e1601659.

(51) Fu, K. K.; Gong, Y.; Hitz, G. T.; McOwen, D. W.; Li, Y.; Xu, S.; Wen, Y.; Zhang, L.; Wang, C.;Pastel, G. Three-Dimensional Bilayer Garnet Solid Electrolyte Based High Energy Density Lithium Metal–Sulfur Batteries. *Energy Environ. Sci.* **2017**, *10*, 1568-1575.

(52) Luo, W.; Gong, Y.; Zhu, Y.; Li, Y.; Yao, Y.; Zhang, Y.; Fu, K.; Pastel, G.; Lin, C. F.;Mo, Y. Reducing Interfacial Resistance between Garnet-Structured Solid-State Electrolyte and Li-Metal Anode by a Germanium Layer. *Adv. Mater.* **2017**, *29*, 1606042.

(53) Liu, B.; Gong, Y.; Fu, K.; Han, X.; Yao, Y.; Pastel, G.; Yang, C.; Xie, H.; Wachsman, E. D.;Hu, L. Garnet Solid Electrolyte Protected Li-Metal Batteries. *ACS Appl. Mater. Interfaces* **2017**, *9*, 18809-18815.

(54) Han, F.; Westover, A. S.; Yue, J.; Fan, X.; Wang, F.; Chi, M.; Leonard, D. N.; Dudney, N. J.; Wang, H.;Wang, C. High Electronic Conductivity as the Origin of Lithium Dendrite Formation within Solid Electrolytes. *Nat. Energy* **2019**, 1.

(55) Chandrasekhar, S. *Hydrodynamic and Hydromagnetic Stability*; Courier Corporation, 2013.

(56) Drazin, P. G.;Reid, W. H. *Hydrodynamic Stability*; Cambridge university press, 2004.

(57) Mukherjee, R.;Sharma, A. Instability, Self-Organization and Pattern Formation in Thin Soft Films. *Soft matter* **2015**, *11*, 8717-8740.

(58) Timoshenko, S. P.;Gere, J. M. *Theory of Elastic Stability*; Courier Corporation, 2009.

(59) Porter, D. A.; Easterling, K. E.;Sherif, M. *Phase Transformations in Metals and Alloys, (Revised Reprint)*; CRC press, 2009.

(60) Bai, P.; Li, J.; Brushett, F. R.;Bazant, M. Z. Transition of Lithium Growth Mechanisms in Liquid Electrolytes. *Energy Environ. Sci.* **2016**, *9*, 3221-3229.

(61) Chen, K.-H.; Wood, K. N.; Kazyak, E.; LePage, W. S.; Davis, A. L.; Sanchez, A. J.;Dasgupta, N. P. Dead Lithium: Mass Transport Effects on Voltage, Capacity, and Failure of Lithium Metal Anodes. *J. Mater. Chem. A* **2017**, *5*, 11671-11681.

(62) Sand, H. J. On the Concentration at the Electrodes in a Solution, with Special Reference to the Liberation of Hydrogen by Electrolysis of a Mixture of Copper Sulphate and Sulphuric Acid. *Proc. Phys. Soc.* **1899**, *17*, 496.

(63) Callen, H. B. *Thermodynamics & an Intro. To Thermostatistics*; John wiley & sons, 2006.

(64) Atkins, P.; De Paula, J.;Keeler, J. *Atkins' Physical Chemistry*; Oxford university press, 2018.

(65) Li, J. C.-M. Physical Chemistry of Some Microstructural Phenomena. *Metall. Trans. A* **1978**, *9*, 1353-1380.

(66) Bazant, M. Z. Theory of Chemical Kinetics and Charge Transfer Based on Nonequilibrium Thermodynamics. *Acc. Chem. Res.* **2013**, *46*, 1144-1160.

(67) Koerver, R.; Zhang, W.; de Biasi, L.; Schweidler, S.; Kondrakov, A. O.; Kolling, S.; Brezesinski, T.; Hartmann, P.; Zeier, W. G.;Janek, J. Chemo-Mechanical Expansion of Lithium Electrode Materials–on the Route to Mechanically Optimized All-Solid-State Batteries. *Energy Environ. Sci.* **2018**, *11*, 2142-2158.

(68) Zhao, K.; Pharr, M.; Wan, Q.; Wang, W. L.; Kaxiras, E.; Vlassak, J. J.;Suo, Z. Concurrent Reaction and Plasticity During Initial Lithiation of Crystalline Silicon in Lithium-Ion Batteries. *J. Electrochem. Soc.* **2012**, *159*, A238-A243.

(69) Xu, R.; Sun, H.; de Vasconcelos, L. S.;Zhao, K. Mechanical and Structural Degradation of Linixmnycozo2 Cathode in Li-Ion Batteries: An Experimental Study. *J. Electrochem. Soc.* **2017**, *164*, A3333-A3341.

(70) Zhang, X.; Shyy, W.;Sastry, A. M. Numerical Simulation of Intercalation-Induced Stress in Li-Ion Battery Electrode Particles. *J. Electrochem. Soc.* **2007**, *154*, A910-A916.

(71) Barai, P.;Mukherjee, P. P. Stochastic Analysis of Diffusion Induced Damage in Lithium-Ion Battery Electrodes. *J. Electrochem. Soc.* **2013**, *160*, A955-A967.
(72) Barai, P.; Huang, B.; Dillon, S. J.;Mukherjee, P. P. Mechano-Electrochemical Interaction Gives Rise to Strain Relaxation in Sn Electrodes. *J. Electrochem. Soc.* **2016**, *163*, A3022-A3035.
(73) Mistry, A.;Mukherjee, P. P. Precipitation–Microstructure Interactions in the Li-Sulfur Battery Electrode. *J. Phys. Chem. C* **2017**, *121*, 26256-26264.
(74) Mistry, A. N.; Cano-Banda, F.; Law, D.; Hernandez-Guerrero, A.;Mukherjee, P. P. Non-Equilibrium Thermodynamics in Electrochemical Complexation of Li–Oxygen Porous Electrodes. *J. Mater. Chem. A* **2019**, *7*, 8882-8888.
(75) Barai, P.; Higa, K.; Ngo, A. T.; Curtiss, L. A.;Srinivasan, V. Mechanical Stress Induced Current Focusing and Fracture in Grain Boundaries. *J. Electrochem. Soc.* **2019**, *166*, A1752-A1762.
(76) Moran, M. J.; Shapiro, H. N.; Boettner, D. D.;Bailey, M. B. *Fundamentals of Engineering Thermodynamics*; John Wiley & Sons, 2010.
(77) Guggenheim, E. A. Thermodynamics-an Advanced Treatment for Chemists and Physicists. *Amsterdam, North-Holland, 1985, 414 p.* **1985**.
(78) Petong, P.; Pottel, R.;Kaatze, U. Water−Ethanol Mixtures at Different Compositions and Temperatures. A Dieletric Relaxation Study. *The Journal of Physical Chemistry A* **2000**, *104*, 7420-7428.
(79) Mistry, A. N.;Mukherjee, P. P. Probing Spatial Coupling of Resistive Modes in Porous Intercalation Electrodes through Impedance Spectroscopy. *Phys. Chem. Chem. Phys.* **2019**, *21*, 3805-3813.
(80) Hill, T. L. *An Introduction to Statistical Thermodynamics*; Courier Corporation, 1986.
(81) Israelachvili, J. N. *Intermolecular and Surface Forces*; Academic press: New York, 2011.
(82) Allen, M. P.;Tildesley, D. J. *Computer Simulation of Liquids*; Oxford university press, 2017.
(83) Liu, X.; Chen, Y.; Hood, Z. D.; Ma, C.; Yu, S.; Sharafi, A.; Wang, H.; An, K.; Sakamoto, J.; Siegel, D. J.; Cheng, Y.; Jalarvo, N. H.;Chi, M. Elucidating the Mobility of H+ and Li+ Ions in (Li6.25−Xhxal0.25)La3zr2o12via Correlative Neutron and Electron Spectroscopy. *Energy Environ. Sci.* **2019**, *12*, 945-951.